applied sciences

MDPI

Article

Seismic Retrofit of Existing Structures Based on Digital Surveying, Non-Destructive Testing and Nonlinear Structural Analysis: The Case of Gjirokastra Castle in Albania

Marieta Núñez García [1,*], Savvas Saloustros [2], Felix Mateos Redondo [3], José Alberto Alonso Campanero [1], Javier Ortega [2], Federica Greco [2], Chrysl Aranha [2] and Irene Martínez Cuart [1]

[1] Proskene—Conservation and Cultural Heritage, 28003 Madrid, Spain
[2] FENEC, 28007 Madrid, Spain
[3] GEA—Asesoría Geológica, 33192 Llanera, Spain
* Correspondence: marieta.nunez@proskene.com

Featured Application: This paper presents a multi-disciplinary scientific methodology for the structural assessment and design of structural interventions on heritage structures. The methodology is based on the use of state-of-the-art non-destructive inspection and structural analysis tools that can help take informed decisions in a restoration and retrofit project.

Abstract: The present paper showcases the work carried out as part of the seismic retrofit of the Ottoman fortress of Gjirokastra, a UNESCO World Heritage site located in Albania. The need for strengthening and retrofitting the structure stems from the fact that it is situated in a region of high seismicity and showed signs of structural distress at the time of investigation. The hill on which the castle is built also has stability issues. The seismic retrofit focused on a damaged stone masonry tower of the fortress and was designed following a comprehensive methodology for the inspection, diagnosis and geotechnical and structural analyses. Through the use of non-destructive tests, the existing soil conditions, the material properties and composition and the dynamic behaviour of the tower were assessed. Nonlinear finite element analysis was used to establish the cause of the existing damage and to determine the most effective strengthening solutions. The findings of the investigation revealed potential causes of the observed damage as well as the need to carry out retrofitting works at the tower beyond ground improvement solutions to bring the performance of the structure up to the code-specified level. This paper highlights the importance of planning and coordination between all the relevant disciplines involved in the project, so that apt inspection and diagnostic tools can be used to fill in the gaps where information is missing and to design optimal and integrated structural interventions in historic structures. Satisfactory seismic performance can be obtained by using a combination of retrofitting techniques, which specifically target the weak elements identified via the analyses.

Keywords: heritage structure; stone masonry; sonic-pulse velocity; dynamic identification; finite element analysis; soil settlements; seismic retrofit; geotechnical investigations; MASW; DInSAR

Citation: Núñez García, M.; Saloustros, S.; Mateos Redondo, F.; Alonso Campanero, J.A.; Ortega, J.; Greco, F.; Aranha, C.; Martínez Cuart, I. Seismic Retrofit of Existing Structures Based on Digital Surveying, Non-Destructive Testing and Nonlinear Structural Analysis: The Case of Gjirokastra Castle in Albania. *Appl. Sci.* **2022**, *12*, 12106. https://doi.org/10.3390/app122312106

Academic Editors: Marco Francesco Funari, Anjali Mehrotra and Daniele Malomo

Received: 27 September 2022
Accepted: 16 November 2022
Published: 26 November 2022

1. Introduction

The conservation and restoration of historical masonry structures comprise a challenging field of study because of the many uncertainties that are involved in determining their material properties and composition, the structural connectivity between portions belonging to different phases of construction, complex geometrical features, geological conditions, etc. Therefore, the assessment of their structural safety is a complex process that requires a thorough multidisciplinary approach that includes, but is not limited to, historical, architectural and archaeological studies, material testing, monitoring, structural

analysis and geotechnical investigation. Since historic masonry structures are particularly vulnerable to seismic loading because of their mass, uncertainties related to the load definition add to the complexity of their safety assessment in seismic areas.

The challenge in designing appropriate structural interventions in historic buildings is that the safety of the structure must be guaranteed, while simultaneously complying with conservation principles, such as the criteria of minimum intervention, compatibility and avoiding superfluous invasive approaches. Similarly, the investigation process also needs to respect the historic character of the structure and adhere to the minimum-intervention criterion. In view of this, the use of qualitative non-destructive inspection and testing complemented by quantitative structural analysis is recommended by common standards and guidelines [1,2]. Despite the many methods of structural analysis available [3], numerical methods based on Finite Element Analysis (FEA) have gained popularity in recent years because of increased computation capability that allows for modelling complex geometry using more realistic material models that can simulate the nonlinear behaviour of masonry. There are many examples in the literature that successfully applied this approach in the analysis of heritage sites around the world [4–9]. In situ experimental campaigns are complementary and requisite to feed numerical models with real data from the structure and provide the means to calibrate and validate numerical models [9–13].

The main objective of the paper is to demonstrate how the integration of advanced inspection and analysis tools from the outset of a historic preservation project and as part of the design process can help in the selection of interventions that are minimally invasive and respectful of the historic fabric, while concurrently upgrading the seismic performance of the structure. This paper highlights the importance of planning and coordination between all the relevant disciplines involved in the project, so that apt inspection and diagnostic tools can be used to fill in the gaps where information is missing and to design optimal and integrated structural interventions in historic structures.

The paper first outlines the applied methodology and introduces the case study. Subsequently, the non-destructive campaign and safety assessment, consisting of both geotechnical and structural investigations, are described. The subsurface (geotechnical) studies focused on assessing the stability of the supporting soil and the analysis of the superstructure included FEA and kinematic analysis. Finally, the paper presents the design approach and the different retrofitting solutions that were considered and analysed in the pursuit of the optimal intervention in terms of safety and respect to the authenticity of the structure.

2. Applied Methodology

The structural assessment followed a multi-step approach, which started out with gathering and verifying data obtained from different sources, such as available documentation, field investigations, in situ measurements and tests, numerical modelling, building codes and standards. Visual inspection, laser scanning, monitoring of environmental conditions and crack widths, sonic testing, ground penetrating radar, drone photogrammetry, damage mapping and material testing were part of the technical tasks carried out to gain a holistic understanding of the tower in its existing condition. Figure 1 summarizes the methodology adopted for the numerical modelling and analysis of the tower.

The geotechnical assessment and strengthening consisted of a detailed characterisation of the different areas of instability of the castle and the adjacent slopes using a combination of in situ and laboratory testing. The tasks carried out included geological mapping, structural geological mapping, geomorphological mapping, preparation of geophysical and geological profiles, analysis of ground displacements with DInSAR (Differential Interferometric Synthetic Aperture Radar), geological risk mapping, slope-stability analysis, FEA and material characterization. The combination of geotechnical and structural field investigations with numerical analysis of the structure in both the current and retrofitted conditions were key to obtain a complete understanding of the underlying causes of damage and to identify the most effective solution to meet performance objectives.

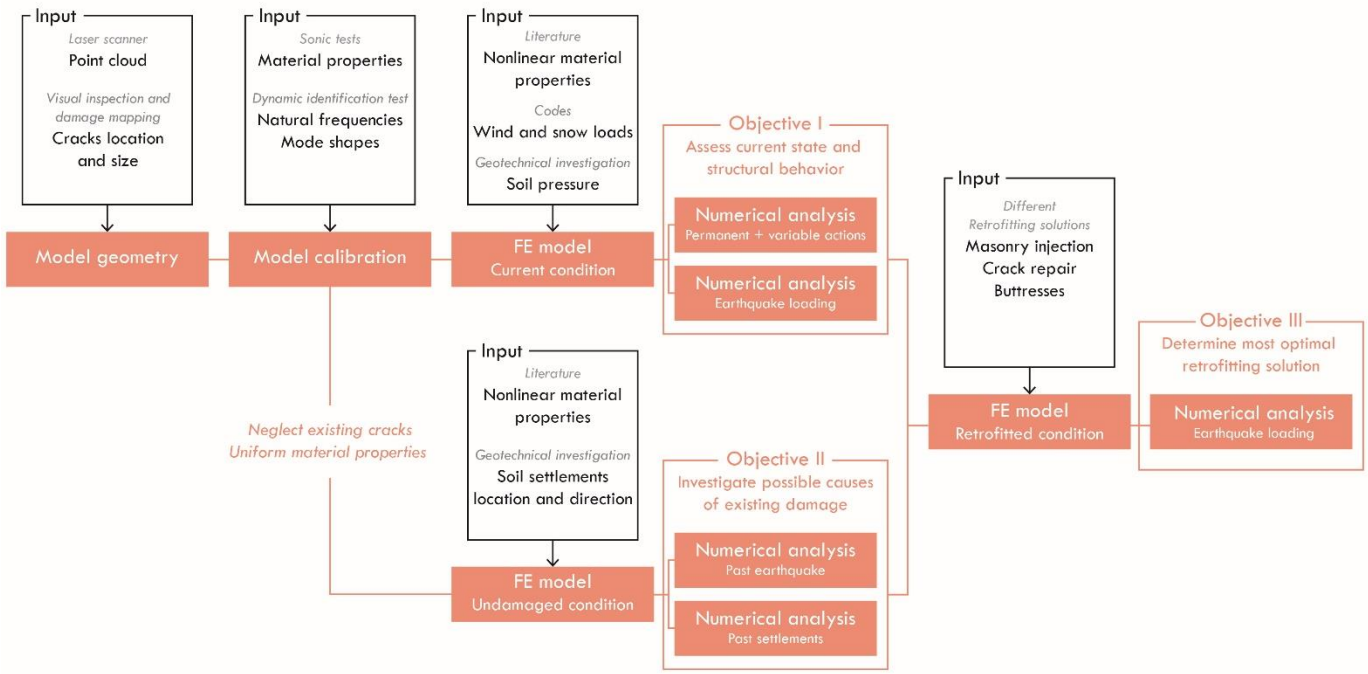

Figure 1. Schematic diagram of the methodology adopted for the numerical analysis and design of retrofitting solution for the structure of the tower.

3. Description of the Building

The castle of Gjirokastra, part of the historic city of Gjirokastra, was inscribed in the UNESCO World Heritage List in 2005 (Figure 2). It is a unique monument, owing to its historical, architectural and structural value. The observation of damage in certain areas of the fortress prompted the need to study these areas more closely and to evaluate the safety of the structure. The preliminary assessment reports, which were commissioned in 2019, concluded that there was a need to carry out additional studies to identify the cause of the damage and prevent further degradation. As a result of this recommendation, the corresponding authorities commissioned the project to a multidisciplinary team that included architects, structural engineers, geological engineers, hydrologists and cultural heritage experts.

The structure subject to investigation is a defensive tower located within the curtain walls in the north-eastern part of the fortress, which served as the secondary line of defence. The tower currently consists of freestanding load-bearing stone masonry walls, but it is thought to have originally been crowned by a vaulted roof, akin to what was observed in another tower of the fortress. Through architectural and historical studies, wall segments belonging to different construction periods were identified: an inner wall enclosure from the 14th–19th C and an external wall enclosure from the 19th C. The tower shows the presence of significant vertical cracks at several locations on its perimeter walls.

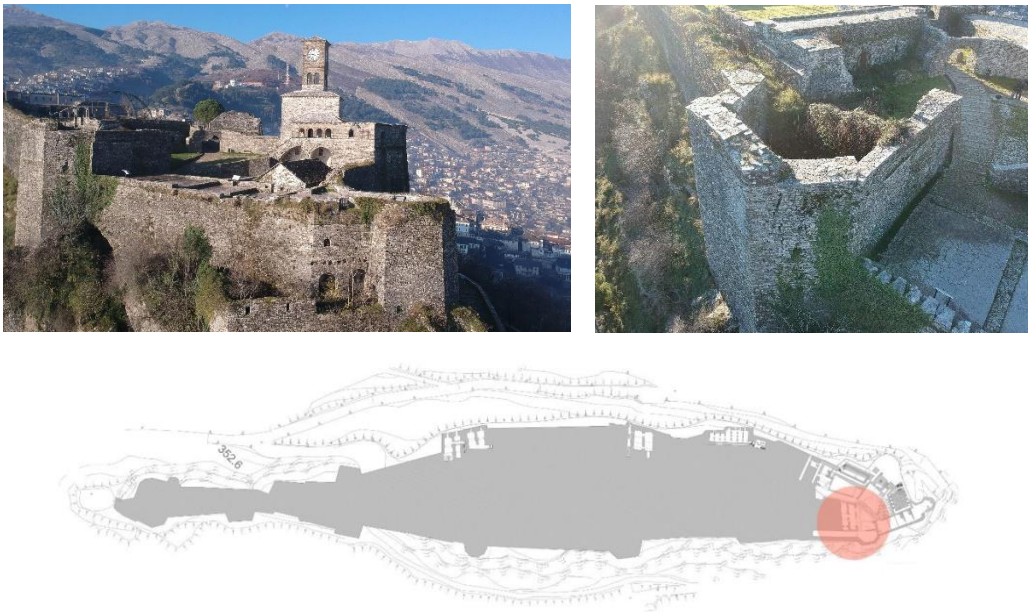

Figure 2. (**Top left**) Aerial view of the north-eastern end of the castle; (**top right**) aerial view of the tower under investigation and location of tower in the fortress, marked with an orange circle (**bottom**) (Photo credit: Rand Eppich).

4. Non-Destructive Investigation

The Non-Destructive Testing (NDT) campaign included the investigation of the subsurface (geotechnical investigations) and superstructure (structural investigations). The tests carried out were complementary to the extensive visual inspection and geometrical survey conducted.

The geotechnical investigation aimed at obtaining detailed geological and geomorphological information on the rocky hill supporting the castle and the adjoining slopes. The focus of the structural investigation was to assess and characterize the inner morphology and the mechanical properties of the masonry elements, as well as the global structural behaviour of the tower.

4.1. Geological and Geotechnical Investigation

The fortress is located atop a narrow confined detritic homoclinal ridge. It is isolated between two narrow valleys, deeply incised in turbiditic successions. The valleys are oriented along the NE-SW axis and the carbonatic bedrock is still intact. Geomorphological processes have given rise to the formation of a narrow and elongated lithostructural surface consisting of relatively more competent rocks (cemented conglomerates) resting on less competent rocks (cementless conglomerates with sand and underlying turbiditic sequences), which are more erodible.

This geological setting has exposed the site to continuous and various types of landslides and predisposes the fortress of Gjirokastra to several types of instability and geological risk: rockfalls and toppling of blocks and complex landslides. Some of the slopes exhibit an advanced degree of retreat/erosion that put the integrity of the castle complex at risk.

4.1.1. Geological, Geotechnical and Geomorphological Maps

The Gjirokastra castle is situated over two geological units: the older Paleogene flysch unit and the younger Pleistocene Conglomerate Unit, which lies above it, as seen in Figure 3, with an angle of discordance over the flysch. The flysch unit has a constant dip direction to the northeast, measuring between 14 and 25 degrees of inclination. Apart from the discordance, no relevant tectonic structure is observed in the study area.

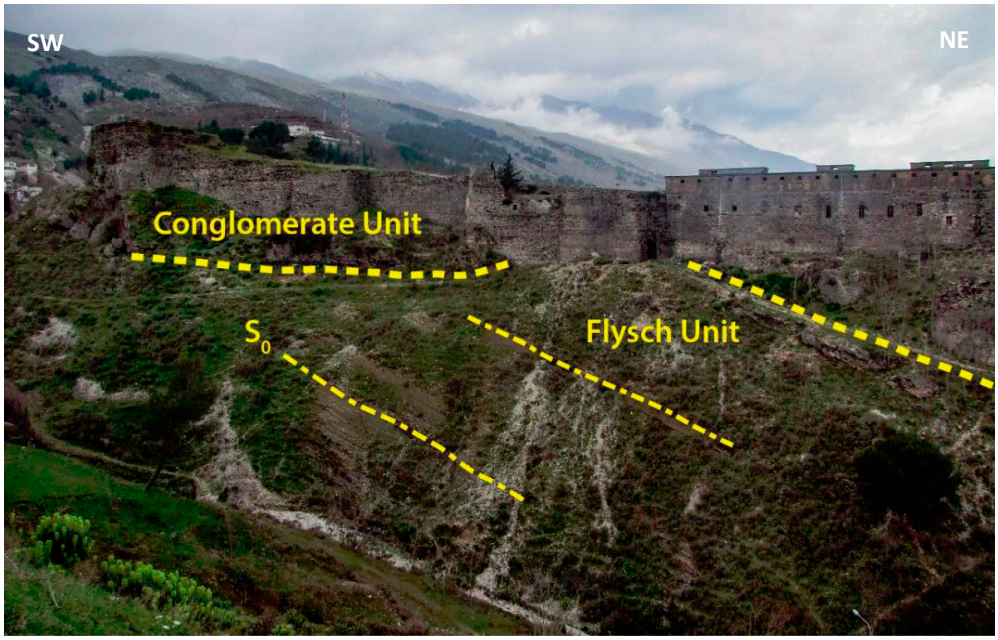

Figure 3. General overview of the southern part of the Gjirokastra castle showing the two geological units.

There are no faults or folds of interest that have been mapped but widespread joints in the geological units can be observed. Some differences between the southern and northern part of the conglomeratic unit are seen (Figure 4). In the southern part, two main families are developed, with subvertical dips and an orthogonal shape with north and west dip directions. In the north section, a third joint family was measured and the dip changes range from east to south.

Figure 4. Detailed image of main joints in the conglomeratic around the tower located at the north-eastern end of the fortress (in red). Blue lines mark the outline of the fortress and the roads below. (Photo credit: GEA, based on photo by Rand Eppich).

A series of geo-mechanical stations was placed on the rocky substrate on which the castle is built and on the surrounding slopes in order to characterize the rock massif

from a geo-mechanical point of view based on its geological–structural field data. This information served as the input data for subsequent FE analyses.

4.1.2. Remote Sensing Analysis: Persistent Scatterer Interferometry (PSI)

The DInSAR technique is a widely used and consolidated geodetic technique based on satellite Synthetic Aperture Radar images. It allows for measuring displacements with millimetric precision. It has applications in different fields, such as geohazard mapping [14] and monitoring, mining, civil engineering or civil protection [15].

The study consisted of a historical analysis of the satellite images of the Gjirokastra castle area. To this aim, two independent Sentinel-1 datasets were processed—in one, 180 images acquired in descending geometry and covering the period between November 2014 and January 2020; in the second one, 140 images acquired in ascending geometry and covering the period between November 2015 and March 2020. The use of both datasets allows one to decompose the measured displacements in the west–east direction and vertical displacements in those areas with intersection. This information enables an easier interpretation of the results compared with the usual single geometry DInSAR results. The results of the DInSAR deformation measurement of the Gjirokastra castle and surrounding area indicated that there have been no significant displacements inside the castle in the last 5 years. More specifically, no displacement was observed at the location of the tower (Figure 5).

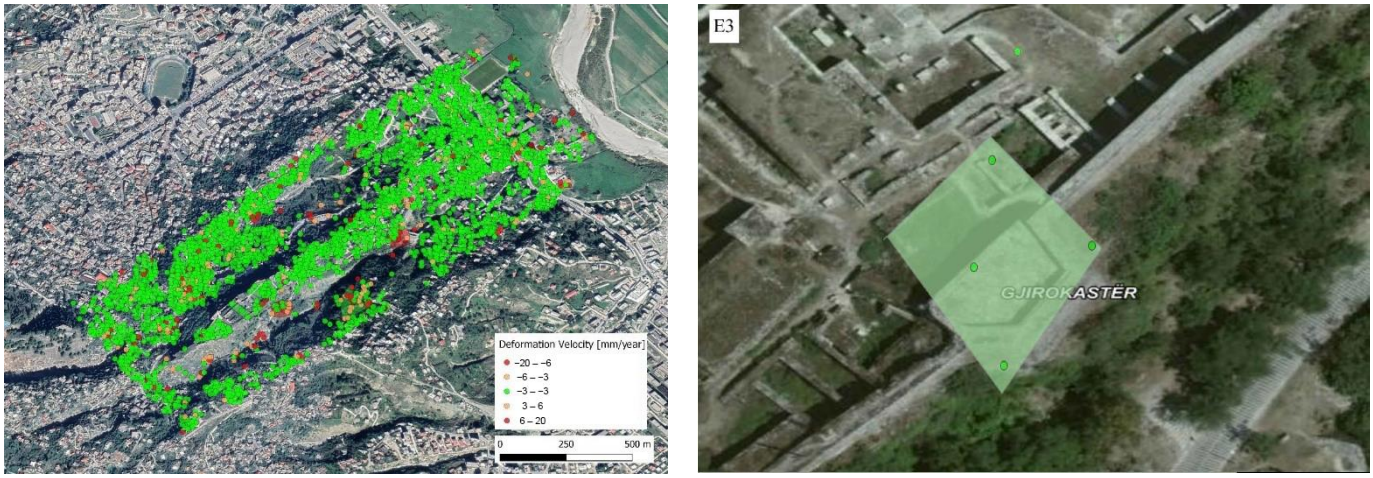

Figure 5. Deformation velocity map of the area of interest (mm/year) (**left**) and around the studied tower (**right**).

4.1.3. Multichannel Analysis of Surface Waves: Seismic Refraction Tomography

Large samples of rotational and translational landslides associated with deposits throughout the castle were not detected. There are only clear samples of some deposits on the eastern slope in the central section of the castle; however, the formation of scarps on the road that encircles the castle is evident, as seen in Figure 6. On this road, one can see the obvious effects of these processes, currently in motion. The scarps have taped morphologies and correspond to a complex system derived from the effect that an infrastructure has on unstable slopes.

Seismic Refraction Tomography (SRT) was used to obtain information on the thickness of the soils on the slopes around the castle and to visualize any detached surfaces due to landslides. A total of 13 SRT measurements was carried out. Three were located within the investigated tower, in the same locations as the Electrical Resistivity Tomography (ERT) profiles (see Section 4.1.4) and the other ten profiles were located on the slopes around the castle (Figure 7). The results of each seismic profile were integrated with the results of the ERT to improve the reliability of the data obtained.

Data acquisition was conducted via a multi-channel seismograph-form DMT model SUMMIT Compact II, equipped with filtration system, reinforcement and digital signal recording and vertical component geophones of 10 Hz. A 5 Kg hammer was used to strike a metal plate of 20 cm diameter to generate the compression wave. An example of the results of SRT is shown in Figure 8.

Figure 6. Scarps along the road on the northwest part of the castle. The retaining wall, as well as the lamppost, are rotated and have sunk with respect to the road. In yellow, dotted lines marking shape and direction of deformation on perimetral road below the castle.

Figure 7. Location of seismic refraction (SRT, in blue) and electrical resistivity tomography (ERT, in red) profiles. (Photo credit: GEA, based on photo by Rand Eppich).

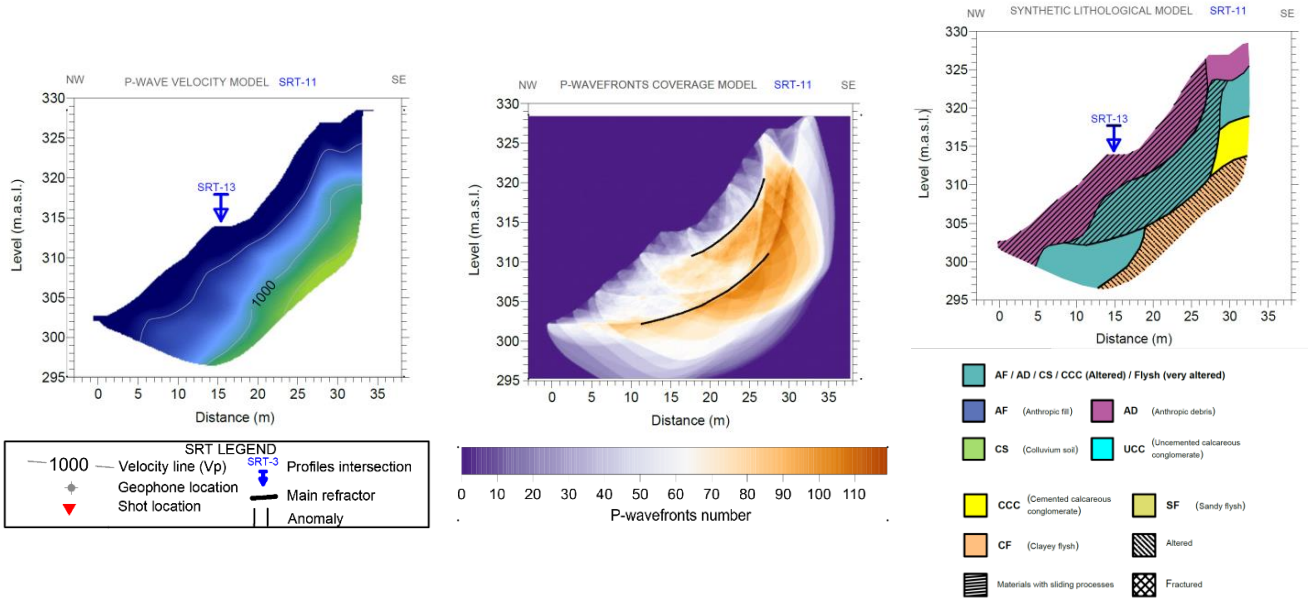

Figure 8. Example of SRT results: P-wave velocity model, P wavefront coverage model and synthetic lithological model obtained for SRT-11.

4.1.4. Electrical Resistivity Tomography (ERT)

ERT was used to obtain information on the geometry of the different soil layers present around the tower, to detect anomalous zones (e.g., cavities) that correspond to instabilities detected in this area of the castle. For ERT data acquisition, a double-injection curve was used with a 256 ms semi-period and readings of potential differences (and, therefore, apparent resistivity) every 2 ms, with an injection curve delay of 250 ms. An average apparent resistivity was obtained at every measurement point from 130 different values, which provided high-quality data readings. The result obtained from the ERT tomography helped to identify the location of a geoelectrical anomaly that corresponds to a cavity under the wall located next to the investigated tower (Figure 9).

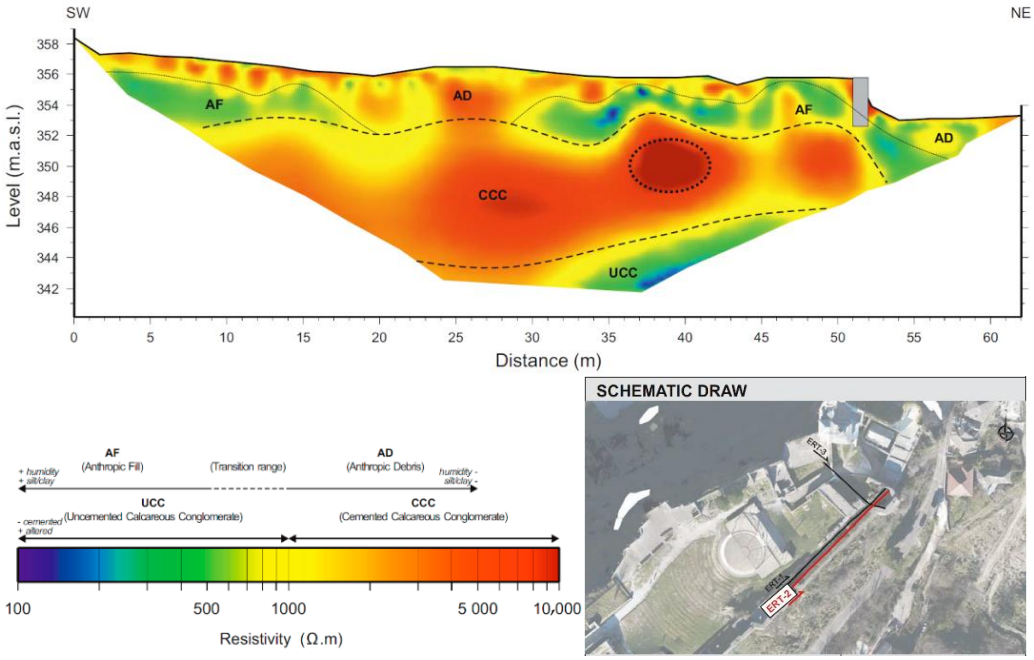

Figure 9. Geoelectrical model obtained for ERT-2. The presence of a geoelectrical anomaly that corresponds to a cavity under the wall located next to the tower is clearly observed. (Photo credit of schematic draw: GEA, based on photo by Rand Eppich).

4.2. Structural Investigation

A combination of UAV (Unmanned Aerial Vehicle) photogrammetry and laser scanning was used for measuring dimensions and identifying damage at inaccessible areas of the castle complex. The NDT works included the mechanical and morphological characterisation of the load-bearing masonry walls of the north-eastern tower using sonic-pulse velocity (SPV) tests and Ground-Penetrating Radar (GPR). Dynamic identification tests using ambient vibration as a source of excitation were also carried out for the characterisation of the dynamic properties of the tower and the subsequent calibration of the numerical models.

4.2.1. Visual Inspection

Visual inspection of the entire castle was carried out to identify and document signs of structural distress. The information that was collected and postprocessed during the historical survey was used to identify the risk level in the different structural elements, depending on the level of damage observed.

Damage mapping was carried out to document existing cracks and identify portions of masonry that were not in good condition. Damage mapping was useful for calibrating the numerical model and it served as a means of comparison with the results of the assessment of the cause of the existing damage.

The existing damage observed at the masonry walls of the tower included cracking, loss of masonry, loss of mortar, lack of structural connection between masonry walls, vegetation growth, unstable and deteriorated wall capping and wall deformation. Masonry loss was observed right above the cavity within the supporting soil, identified by the geotechnical investigation (Figure 9).

4.2.2. LiDAR

Laser scanning data were gathered on site from 111 stations throughout the interior and the exterior of the castle. A laser BLK-360 by Leica Geosystems was used for data acquisition, Cyclone Register 360 was used for point cloud merging and Recap Pro was used for point cloud postprocessing. The geometrical survey was useful to model different walls, as well as to estimate the foundation depth based on the conglomerate level.

Deformation analysis of the external surfaces of the main masonry walls of the tower was carried out by postprocessing the laser-scanner-generated point clouds and relative out-of-plane displacements were plotted on selected masonry walls (Figure 10). The results were used to obtain a better understanding of the out-of-plane displacements in the tower. This input was crucial to understand the effects of past cracking, the relative position between different sections of walls and for interpreting the modal shapes obtained from the dynamic identification.

While some of the relative displacements were more clearly associated with cracking phenomena, others could be related to plumbing from different construction phases or differential masonry degradation and washed-out joints.

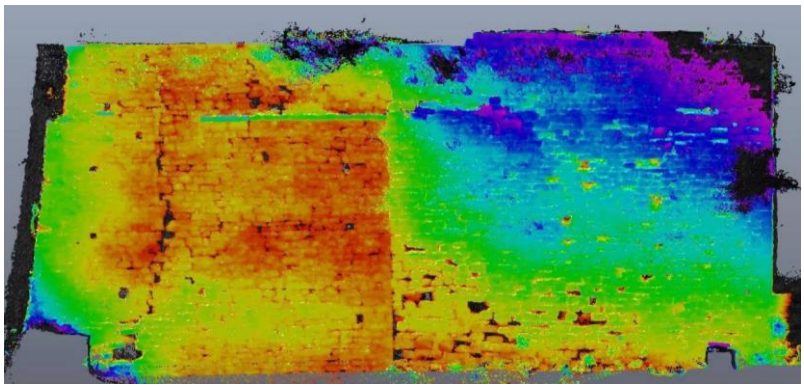

Figure 10. Out-of-plane deformations of the northern elevation of the tower obtained through processing the LIDAR point cloud. The spectrum colour scale indicates the distance of each point to a reference plane, having red colours indicate areas farther away from the plane and purple areas being the closer ones.

4.2.3. Drone Photogrammetry

Aerial drone photographic survey and photogrammetric analysis were carried out by Rand Eppich as part of the surveying campaign, which was key to obtain data in locations that were inaccessible due to steep terrain or overrun with vegetation. The photographic survey was postprocessed to create a photogrammetric model, from which 2D elevations and plans, a 3D meshed model and 2D topographic curves were generated.

4.2.4. Material Sampling and Testing

Samples of stone and mortar were collected from the site from loose units to carry out characterization tests. The outer and inner sides of the castle's walls are built with white limestone for the most part and greyish-brown sandstones to a lesser extent. There were a few areas where conglomerate and a pinkish limestone were observed. It is understood that the latter may have been used in prior interventions. Tests carried out on the

stones aimed to obtain information regarding colorimetric parameters, ultrasonic P-waves velocities, uniaxial compressive strength, porosity, density and specific surface.

The tested value of the uniaxial compressive strength of the white limestone sample was 158.3 ± 21.8 MPa, while the two samples of grey-brown sandstone had compressive strengths of 68 ± 12 Mpa and 8.9 ± 4.1 MPa, respectively. The mortar samples collected in the tower were mostly lime based, except for one, which was cement based.

4.2.5. Monitoring

Monitoring was carried out at the tower to determine the presence of ongoing movement. Three types of monitoring devices were installed: sensors for environmental conditions, manual crack-width monitors and a digital crack-width monitor.

Digital monitoring of the main crack that runs vertically along the tower (seen propagating vertically on the left in Figure 10) was carried out for an approximate duration of 13 months. Average temperatures fluctuated between 8 °C and 26 °C and relative humidity (RH) between 52% and 85% during the period of study, while crack-width variation fluctuated between −1.051 mm and +0.425 mm (Figure 11). The temperature and relative humidity values presented along with the crack-width variation are monthly averages for the city of Gjirokastra. Negative and positive values of crack-width variation indicate closing and opening of cracks, respectively.

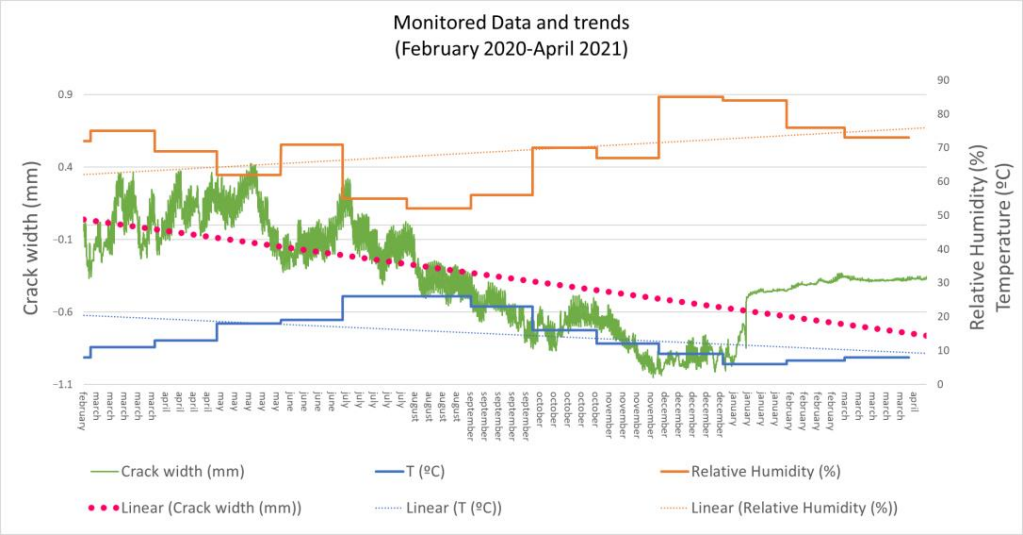

Figure 11. Graph showing variation in monitored parameters from February 2020 to April 2021. Positive values indicate that the crack has closed since the beginning of the monitoring, and negative values indicate that the crack has opened.

A sudden change in the crack width was detected between 8:00 and 9:00 a.m. of local time in Gjirokastra on 12 January 2021. This coincided with a seismic event registered by several seismological institutions, such as the National Observatory of Athens and the European Mediterranean-Seismological Centre. The movement was evidence of the tower and/or conglomerate being vulnerable to seismic events and, therefore, signalled a need for intervention to avoid further propagation of damage or potential collapse in the case of seismic events with higher magnitudes.

4.2.6. Sonic-Pulse Velocity Tests

SPV testing was used to provide a qualitative assessment of the masonry and to obtain quantitative values of mechanical parameters, such as Poisson's ratio (ν) and dynamic modulus of elasticity (E_d), based on the measured wave velocities [16,17]. Given the visible heterogeneity in the morphology of different sections of the tower, all walls were tested at three different heights, as seen in Figure 12. The average velocity of the primary (P)

waves obtained from sonic testing was 1300 m/s, resulting in an average dynamic modulus of elasticity ranging between 2.72 and 3.32 GPa. The P-wave velocities varied between 350 m/s and 2500 m/s. As there was no variation in the masonry typology within the tower, low velocities correspond to very irregular masonry, with a high percentage of voids within the cross section, while higher velocities indicate a more regular, solid masonry wall. The notation of the walls of the north-eastern tower is seen in Figures 12 and 13, which presents the variation in the mean value of the dynamic modulus of elasticity in different portions of the tower.

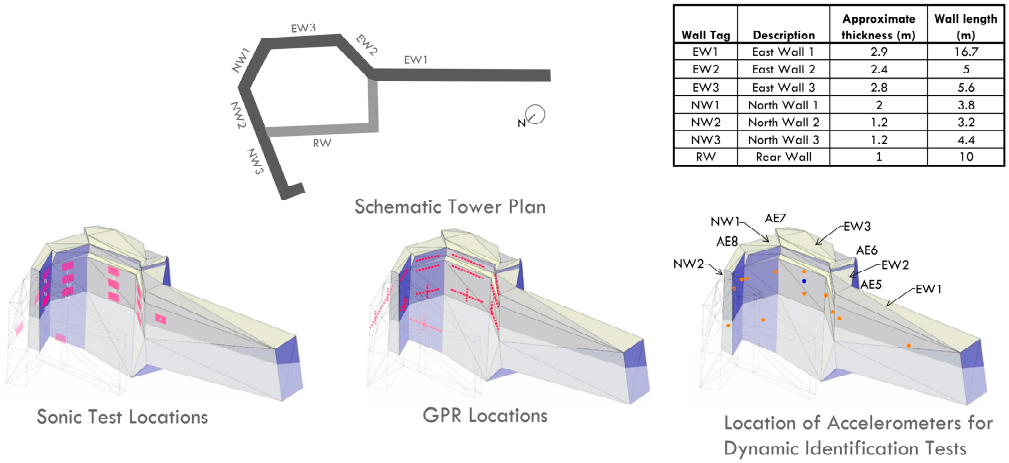

Wall Tag	Description	Approximate thickness (m)	Wall length (m)
EW1	East Wall 1	2.9	16.7
EW2	East Wall 2	2.4	5
EW3	East Wall 3	2.8	5.6
NW1	North Wall 1	2	3.8
NW2	North Wall 2	1.2	3.2
NW3	North Wall 3	1.2	4.4
RW	Rear Wall	1	10

Figure 12. Location of non-destructive tests carried out at the tower.

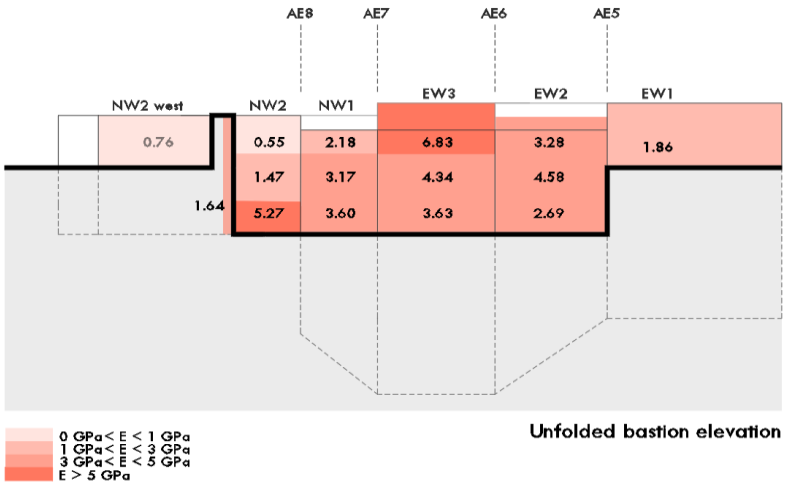

Figure 13. Unfolded tower elevation showing mean E_d values calculated.

Walls NW1-EW3-EW2 have similar mechanical parameters, with the highest dynamic modulus of elasticity measured at the topmost level of the central wall (EW3), possibly confirming the conjecture that this part of the wall is a later addition to the structure. Although the curtain wall on the southern side of the tower (EW1) and the perpendicular wall connected to the northern side of the tower (NW2) had similar mechanical parameters, they were noticeably lower than the ones obtained at walls NW1-EW3-EW2. Similar mechanical parameters obtained in tests conducted at different locations could indicate common construction or intervention dates, matching construction quality or, possibly, a matching state of degradation. At the northern wall orthogonal to the tower (NW2), both direct and indirect sonic tests were carried out. Velocities obtained from the direct tests were higher than the velocities obtained with indirect tests. This could be an indicator of

a consistent material present throughout the whole section of this wall and the absence of a differentiated internal core.

4.2.7. Ground-Penetrating Radar (GPR)

To complement the information obtained from the SPV tests, horizontal and vertical GPR scans were performed at the same locations, see Figure 12. The equipment used for performing the tests was the MALA CX (Concrete Explorer) unit with a 1.2 GHz antenna. The results indicated a similar type of masonry throughout the fortress. The radargrams revealed that the cross-section of the walls was composed of stones of various sizes that are fairly regular, with joints that are mostly horizontal. Based on the reach of the GPR antenna, this morphology extends to a depth of at least 1 m. The thickness of the outer leaf of the walls was found to vary significantly between 10 cm and 40 cm.

Most of the walls that were tested show an overall lack of mortar and the presence of gaps at the interfaces between stones. However, despite the presence of gaps at the interfaces and the generalized lack of mortar in the inner joints, the uncracked walls were found to be in good overall condition. The use of stones within the core results in notably solid walls and could justify the obtained high sonic velocities. Figure 14 shows an example of horizontal scans performed at one of the tower walls. Strong irregular reflections are observed at different depths throughout the thickness, confirming the irregular internal masonry arrangement with gaps at the interfaces and lack of mortar.

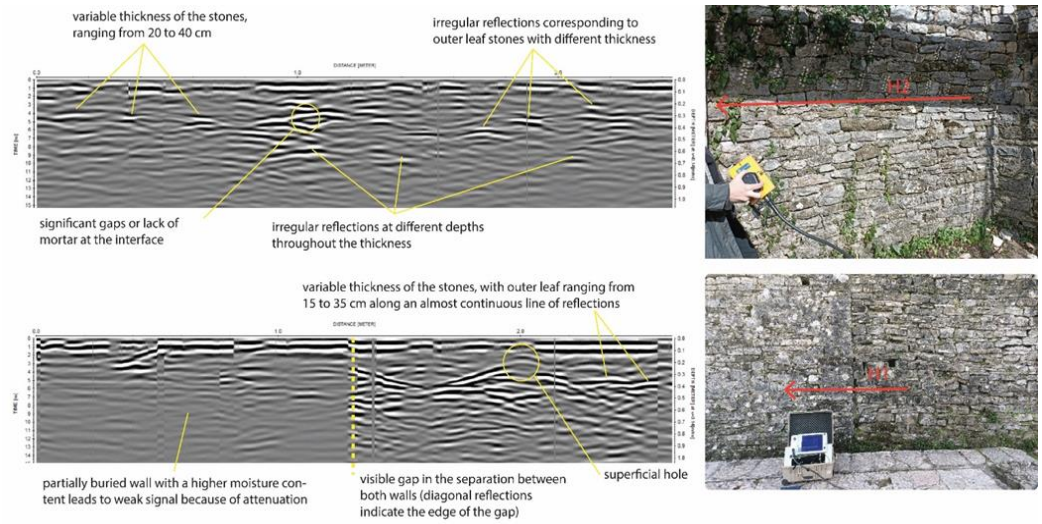

Figure 14. Horizontal GPR scans carried out at different locations in one of the tower walls.

4.2.8. Dynamic Investigation

Dynamic identification tests are useful to obtain the natural frequencies and mode shapes of the structure by measuring structural vibrations due to ambient forces. Accelerometers were located at 14 locations in the middle section of the different walls of the tower (Figure 12), mostly intending to capture expected out-of-plane modes. Three accelerometers were deployed along the height of wall EW3.

Four natural modes of vibration of the structure and associated frequencies were identified (Figure 15). It is acknowledged that the modes captured may include the effects of soil–structure interaction. Past studies measured accelerations at the bottom of the structure as a way of filtering the effects from the soil on the structure's response [18,19]. However, it is noted that no accelerometer could be placed at the base of the wall because the wall extends several meters below the ground on the interior side and the exterior part is inaccessible. To gain confidence that the modes measured capture only the behaviour of the tower, the mode shapes and frequencies were estimated using two different techniques: Enhanced Frequency Domain Decomposition (EFDD) [20] and Stochastic Subspace Identification

(SSI) [21], implemented in the ARTeMIS software [22]. The four modes were identified using both methods and the mode shapes were compared on the basis of the Modal Assurance Criterion (MAC). MAC is a statistical indicator that ranges between 0 and 1, with 1 indicating fully consistent mode shapes [23,24]. The MAC values for the mode shapes obtained using the two techniques ranged between 0.88 and 0.98, confirming that the four measured modes are independent of the estimation method used to obtain them.

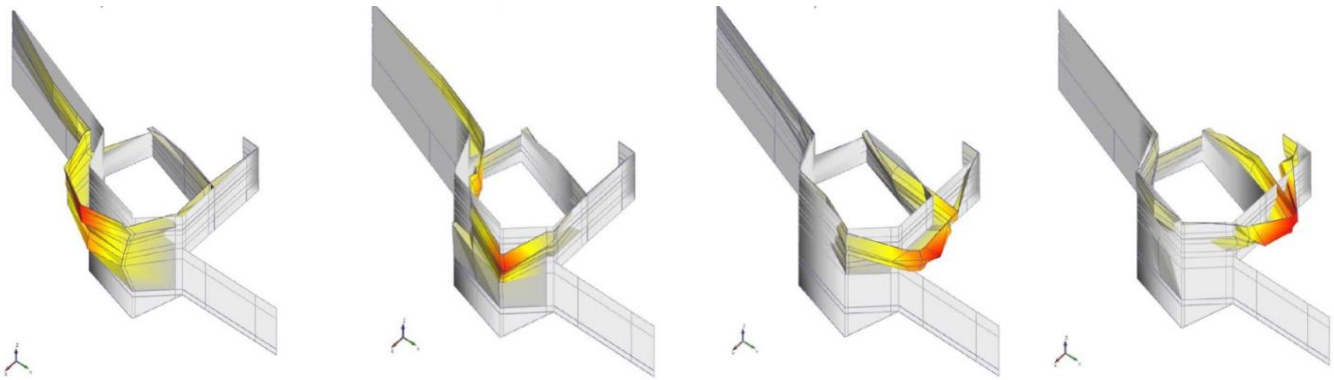

Mode 1 (4.92 Hz) Mode 2 (6.85 Hz) Mode 3 (9.57 Hz) Mode 4 (12.39 Hz)

Figure 15. Mode shapes and natural frequencies of the first four modes identified in the tower.

The first mode corresponds to the out-of-plane movement of the eastern wall EW3. The second mode involves the movement of the corners between NW1-EW3 and EW2-EW1, with a north-to-south out-of-plane movement. Mode-3 corresponds to the out-of-plane movement of the intersecting corner between NW1 and NW2. Finally, Mode-4 corresponds to the out-of-plane movement of NW2 and its extension to the west. The modes obtained reflect the influence of existing cracks in the structural behaviour of the tower, since all of them are local modes involving different parts of the masonry. Although the cracks facilitate the out-of-plane movement of the different walls of the tower, the results indicate that the disconnection between the walls caused by their presence is not total.

5. Safety Assessment

Following the geotechnical and structural NDT investigations, a structural assessment of the tower was carried out. The geological–geotechnical assessment investigated the stability of the supporting soil and potential solutions for retrofit. The main objective of the structural assessment was two-fold. First, the analyses aimed to assess the structural safety of the tower under permanent, variable and seismic actions. Secondly, analyses were carried out to assess the current structural damage and determine whether the existing structural distress observed was caused by past earthquakes or soil settlements. The assessment was carried out using detailed finite element (FE) modelling and kinematic analysis.

5.1. Geological–Geotechnical Assessment

Modelling of the soil as continuum using FEA is suitable for the analysis of soil slopes, massive intact rock or healthy-jointed rock masses. In this work, the commercial FEM software CIVILFEM was used to study the soil stability.

5.1.1. Slope Stability Analysis

Based on the information obtained in the field and lab analyses, a geological risk map was developed to understand the potential landslides and flows that may occur on the slopes surrounding the Gjirokastra castle (Figure 16).

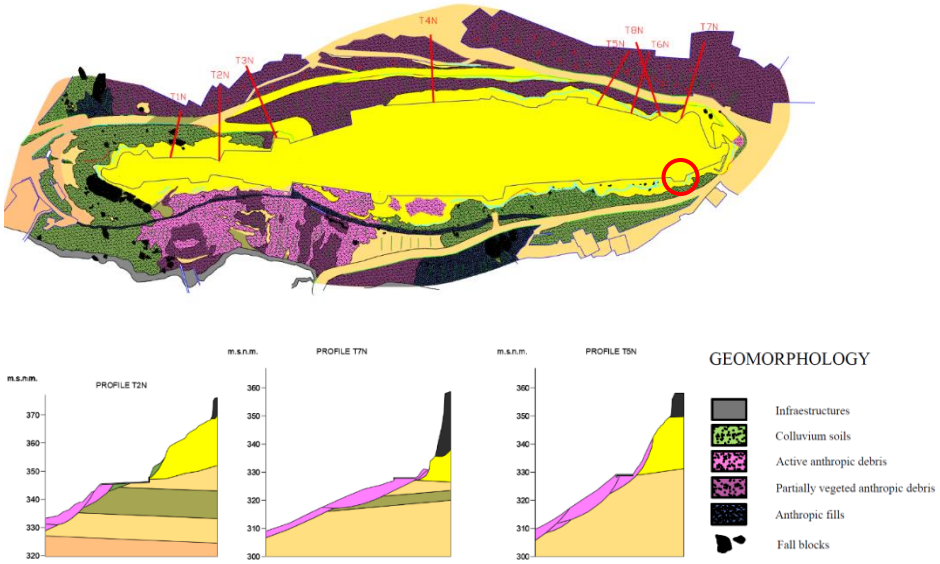

Figure 16. Geomorphological map of the castle area and several examples of geological–geomorphological profiles. The red circle indicates the location of the tower.

FEM stability analysis of the slopes was carried out to propose suitable solutions in the area's housing. The analyses showed that in some areas around the castle, the slopes below the road had significant deformations and there is a high risk of landslides (Figure 17). It was deemed necessary to engineer a solution to stabilize the base of the hillside and minimize the risk to the houses present at the foot of the hills. None of these locations were located directly below the tower, where cliff stability analysis was performed instead.

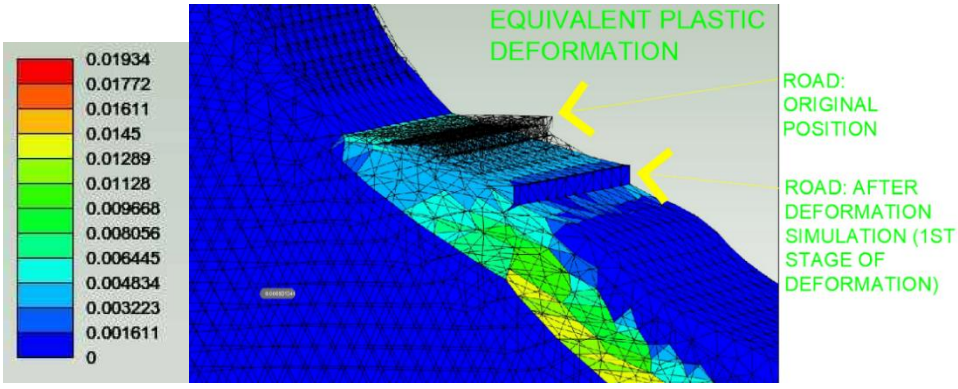

Figure 17. Equivalent plastic deformation obtained by FEM for a small section of the road that surrounds the Gjirokastra castle.

5.1.2. Cliff Stability Analysis

Based on the previous information, the geological–geotechnical stability of the area of the site supporting the castle was studied. A qualitative risk level was assigned to the different sections of the wall based on the probability of failure in the geological substrate and its potential impact on the supported wall. A total of four areas of extreme risk was identified, one of them being located directly below the studied tower. Figure 18 shows an example of the methodology followed based on FEM analyses.

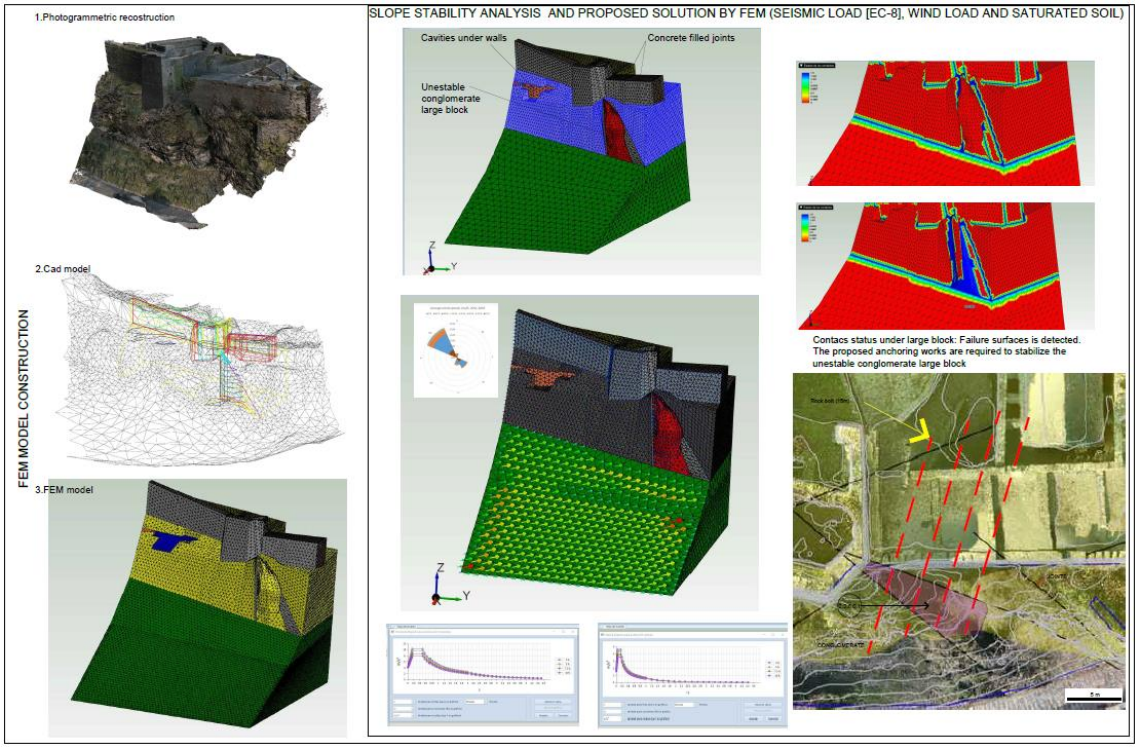

Figure 18. Example of FEM analysis carried out to evaluate and design an engineering solution to stabilize unstable rock blocks. (Photo credit: GEA, aerial photo by Rand Eppich).

The cliff stability analysis revealed that there is a high risk of rock toppling and the potential for rock fall due to the roots of the trees growing in open joints and rotational and/or translational landslides (Figure 18). In the southwestern end of the tower, an open fracture under the wall continued below the castle. In the north-eastern end of the tower, a big fracture under the masonry was observed.

5.2. Structural Assessment

The seismic assessment was carried out per Eurocode [25], since a literature review [26] and preliminary comparative analyses found it to be more conservative than the local Albanian Seismic Code KTP-N.2-89 [27]. The simulation of seismic actions acting on the structure was conducted by means of kinematic and nonlinear static (pushover) analysis. The performance of the structure at each one of the directions was assessed by means of the N2 method, a displacement-based approach proposed by [28], and implemented in various codes, such as Eurocode 8 [25]. This is a seismic assessment method that consists of estimating the demand of the maximum displacement (i.e., the target displacement, d'_t) on the structure for the design earthquake corresponding to the site class and seismic risk characteristics of the site (i.e., Gjirokastra) and comparing it with the displacement capacity of the walls (d'_u). The capacity of the structure was obtained through the pushover analyses, while the seismic demand was defined in Acceleration-Displacement Response Spectrum format according to Annex B of Eurocode 8 [25].

In addition to the seismic loads, the seismic assessment considered wind and snow loads to validate the model, with the fundamental combination specified in Eurocode EN 1990 Basis of Structural Design [29] and the verifications were carried out for the Near Collapse (NC) requirements. Due to the cultural significance of the building, an importance factor $\gamma_I = 1.4$ was applied to estimate the design ground acceleration $a_g = 0.5842$ g for a reference peak ground acceleration $a_{gR} = 0.416$ g, considering a probability of exceedance of 2% in 50 years and a life expectancy of 50 years. The evaluation was carried out for both Type 1 and Type 2 spectra. The site class was determined based on the wave velocities obtained from the

geological NDT testing campaign. The correlation proposed by Brocher [30] was used to obtain the average shear wave velocities for the different soil strata, resulting in category B for the conglomerate and category A for the flysch.

5.2.1. Kinematic Analysis

Kinematic analysis is commonly used in masonry buildings to study local collapse mechanisms that might take place within a structure under seismic loads because of loss of equilibrium. Visual inspection, deformation analysis and study of the existing damage, i.e., cracking pattern, are important to identify and analyse potential collapse mechanisms.

In-plane and out-of-plane local overturning collapse mechanisms were studied in terms of equilibrium analysis in two different ways: a simplified way in which the seismic load activating the collapse is estimated in terms of seismic acceleration and a seismic multiplier (linear kinematic analysis) and a more precise way in which the seismic load triggering the collapse is estimated in terms of seismic displacement (nonlinear kinematic analysis). The method was particularly helpful as a preliminary analysis for assessing the comparative vulnerability of different elements and serving as a basis to prioritize the interventions to be studied and the need for advanced numerical modelling. Several collapse mechanisms were, therefore, studied throughout the castle, including the tower subject to study in this paper.

For the analyses performed, each macro-element was considered a rigid block, with no tensile resistance at the connection to adjacent macro-elements. Limited compressive strength of masonry was taken into account by considering an updated location of hinge formation at the rotation point/axis. Results indicated that the most vulnerable collapse mechanisms were those involving slender walls, possibly corresponding to the 14th–19th C curtain wall configuration. Figure 19 shows some of the different kinematisms studied. The kinematism presented in the third column from the left was found to be the most vulnerable.

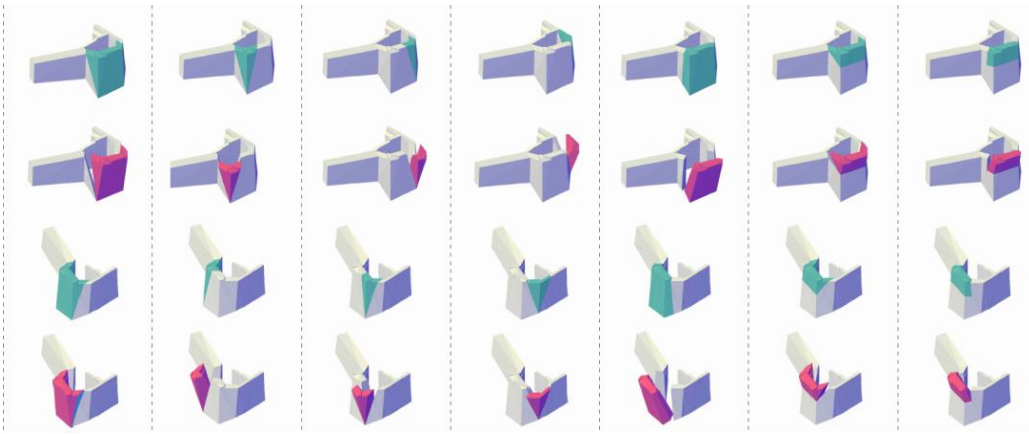

Figure 19. Three-dimensional representation of some of the kinematisms studied at the tower. Macro-elements involved in the kinematism are shown in the original position (green) and rotated position (red) for illustrative purposes.

5.2.2. Numerical Analysis

The geometry of the FE model of the tower was prepared based on the point cloud obtained via laser scanning, while information on the soil strata and properties were obtained from the geotechnical investigations.

FE Model Generation

The walls of the FE model were geometrically defined in terms of: (a) overall geometry of load-bearing masonry walls; (b) subsections of masonry having different material properties; and (c) large existing cracks. The sections of the walls having different material

properties were defined based on the results of the NDT campaign and in correlation with the in situ visual inspection and aerial photogrammetry. Cracks were incorporated in the model as 10 cm wide full-height solid elements, splitting the walls almost vertically. The geometry of the cracks was simplified to match their predominant direction in the actual structure. The walls were assumed to extend up to the depth of the strata of conglomerate identified in the geotechnical investigations.

The model was discretized using 120,389 isoparametric tetrahedral elements based on linear interpolation and Gauss integration, with a maximum size of 0.5 m. The following modifications were made to the geometry to capture a more realistic structural response and shorten the computational time: (a) reduction in the length of wall EW1 and (b) replacement of the small transversal wall between EW1 and RW with the corresponding boundary conditions on the walls adjacent to it. The final geometry of the structure is presented in Figure 20. The base of the model was fixed in all analyses, except for the soil settlement study. The horizontal movement orthogonal to sections of walls EW1 and NW1 was restrained at locations in contact with the neighbouring walls, simulating the boundary conditions imposed by those elements.

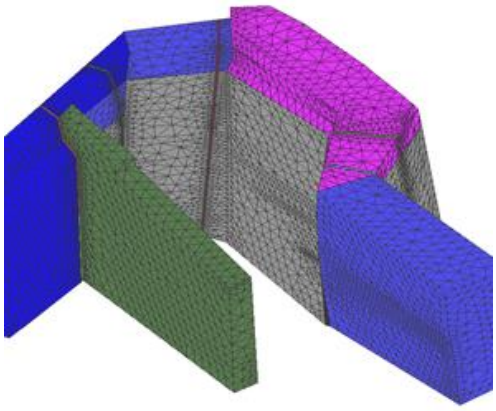

Figure 20. The finite element model of the investigated tower, where different colours correspond to areas where different material properties were assigned (see Figure 21).

Model Calibration

The calibration of the numerical model is carried out by comparing the natural frequency and modal shape of each mode with the experimental one. Numerical and experimental frequencies are compared in terms of absolute error, while modal shapes are compared using the MAC.

The results of the SPV tests were used to categorize the masonry into five different types on a qualitative basis. The zones can be identified in Figure 21. The maximum values of E_d for each of the above masonry types are shown in Figure 13.

The following labelling of the cracks is adopted hereafter, with reference to Figure 21:

- Crack-1: Crack at EW2, with one end at the corner between EW1 and EW2.
- Crack-2: Crack at EW2, close to the corner between EW2 and EW3.
- Crack-3: Crack at NW1, close to the corner between NW1 and EW3.
- Crack-4: Crack at NW2, close to the corner between NW1 and NW2.
- Crack-5: Construction joint/crack at NW2, separating NW2 and NW3.

All cracks were separated into two segments along their height, with the first corresponding to visible cracks, as identified from the in situ inspection, and the second to the portion of the crack that extends into the base of the wall. Initially, the cracks were assigned the same properties as the adjacent masonry. During the model calibration procedure, the stiffness of the cracks was reduced to calibrate the model based on the recorded mode shapes and frequencies. It is acknowledged that other parameters in addition to the crack stiffness (e.g., soil–structure interaction or Young's Modulus for the different types of

masonry) could also be incorporated in the calibration process. However, based on the data gathered from the various in situ tests performed, the influence of the cracks was considered to be the parameter with the highest influence.

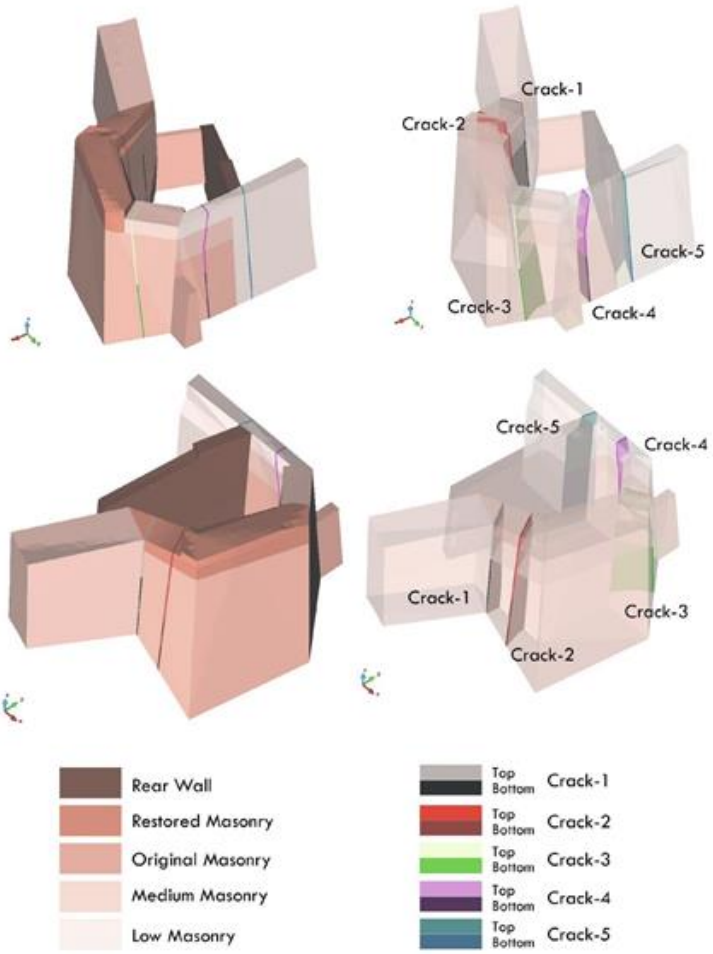

Figure 21. Model of the simulated tower showing the location of the different types of masonries and cracks.

Table 1 presents a comparison between the experimental and numerical modal frequencies for the four experimentally identified modes along with the corresponding MAC values. The computed modal frequencies for all the modes are very close to the experimental ones, with a relative error between the numerical results and the average of the different test setups equal or lower than 2% for all cases. The high MAC values indicate a good correlation between the computed modal shapes and the ones identified by the analysis of the dynamic identification results. It is noted that the calibration of a numerical model of an existing structure with significant damage is not trivial, and the calibration procedure can be based on a single mode representing the most vulnerable part of the structure [31]. In this case, a very good representation of the tower's dynamic response by the numerical model is achieved due to the detailed information on the geometry and crack locations provided by the laser scanning survey as well as on the material properties, masonry quality and dynamic behaviour obtained from the non-destructive experimental campaign. Figure 22 presents the experimental and numerical modal shapes for Modes 1 to 4.

Table 1. Frequencies and MAC values of the four modes obtained through the dynamic identification campaign and numerical modal analysis.

	Experimental Range of All Setups	Numerical Model	Absolute Error in Frequencies	MAC
Modes	**Freq. [Hz]**	**Freq. [Hz]**	**[%]**	**[-]**
Mode 1	4.92	4.82	2.03	0.88
Mode 2	6.85	6.88	0.44	0.78
Mode 3	9.57	9.54	0.31	0.75
Mode 4	12.39	12.42	0.24	0.75

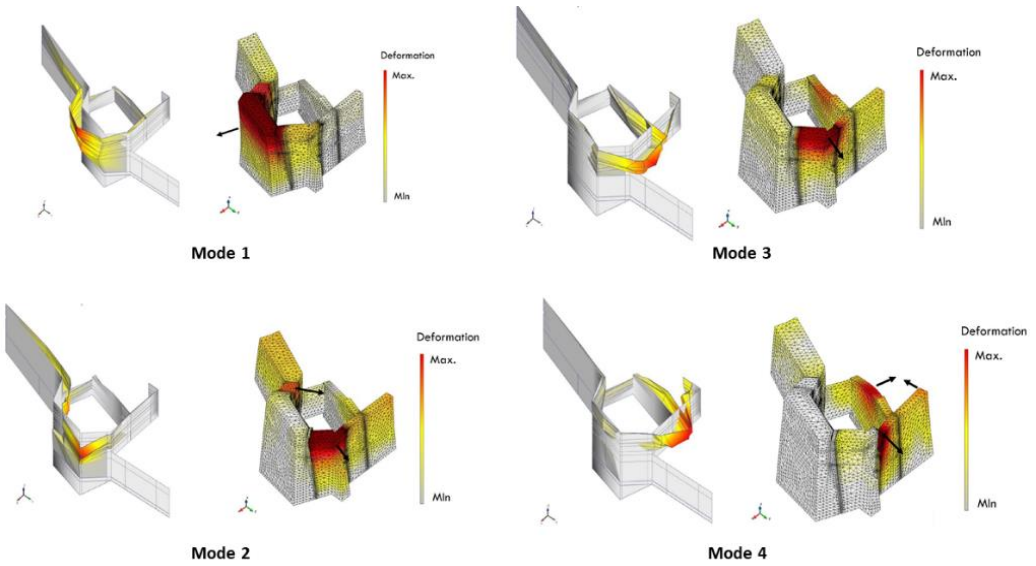

Figure 22. Comparison of experimental (dynamic identification) and numerical (eigenvalue analysis) modal shapes. Black arrows in the numerical results indicate the direction of movement.

The elastic properties of the final model are presented in Table 2. The ratio between the value of the dynamic Young's Modulus (computed through the sonic-pulse velocity tests) and the final selected value varies between 1.0 and 1.4 for the different masonry typologies and is in agreement with the values for quasi-brittle materials reported in the literature [10,32,33]. A Young's Modulus of 0.4 Mpa was used for all cracks, except for Crack-5 and the bottom part of Crack-2. This implies that the at cracks 1–4, the stiffness is much lower but there is a level of interconnection between the adjacent walls. The elastic properties used at the location of Crack-5 are much higher than the other cracks, referring to a closed crack at the base with smaller degradation at the top.

Material Properties

Table 2 presents the material properties assigned to the different masonry zones and cracks. The compressive strength (f_c), defined in Equation (1), considers a linear relationship with the Young's Modulus, E, where the coefficient α was taken as 550, in line with recommendations for historic masonry structures [34,35]. The tensile strength (f_t) was assumed as 5% of the compressive strength [35]. A Poisson's ratio of 0.2 was adopted for all materials.

$$E = \alpha f_c \quad (1)$$

The nonlinear mechanical behaviour of the masonry was simulated using a continuum damage mechanics model with damage-induced orthotropic behaviour along the principal axes [36,37] implemented in an in-house FE software. The model uses two distinct damage indices to distinguish between tensile (i.e., cracking) and compressive (i.e., crushing) damage, taking values between 0 (undamaged state) and 1 (completely damaged state).

The tensile response is characterized by a linear part until reaching the peak strength and the post-peak part is defined by an exponential softening law. For the compressive damage, the constitutive law presented in [38] is adopted, allowing for a parabolic hardening–softening part followed by exponential softening. The value of the fracture energy in tension (G_{ft}) and compression (G_{fc}) is obtained from Equation (2) and Equation (3), respectively [35].

$$G_{ft} = 0.04 f_t^{0.7} \quad (2)$$

$$G_{fc} = 1.6 f_c \quad (3)$$

Table 2. Material properties of the different qualities of masonry considered in the numerical model.

Material	E (N/mm^2)	f_c (N/mm^2)	f_t (N/mm^2)	G_{fc} (N/mm^2)	G_{ft} (N/mm^2)	ρ [kg/m^3]
Masonry 1 "Original"	2600	4.70	0.240	7.6	0.015	2100
Masonry 2 "Medium"	1400	2.55	0.130	4.1	0.009	2000
Masonry 3 "Low"	700	1.27	0.065	2.0	0.006	1900
Masonry 4 "Restored"	3600	6.55	0.320	10.5	0.018	2100
Masonry 5 "Rear Wall"	2200	4.00	0.200	6.4	0.013	2000
Cracks 1, 3, 4	0.4	-	-	-	-	1000
Crack 2 top	0.4	-	-	-	-	1000
Crack 2 bottom	2.0	-	-	-	-	1000
Crack 5 top	100	-	-	-	-	1900
Crack 5 bottom	700	-	-	-	-	1900

Damage Assessment

In order to investigate the cause of the existing structural distress, the original undamaged structure was simulated by a model without any cracks, and uniform material properties corresponding to the "original masonry" type presented in Table 2 were assigned to all the walls. The rear wall of the tower was found to be the most vulnerable element in three out of the four directions under analysis, dictating the failure in the pushover analyses. However, the most significant cracks observed during the visual inspection were located on the outer walls of the tower. Therefore, the rear wall was removed from the model to focus on the effect of a horizontal seismic load on the outer walls.

To determine if the existing damage was caused by past seismic events, nonlinear static pushover analyses were carried out (Figure 23 top). Damage at the top corner between the northern walls, at the location corresponding to the low-quality masonry that currently shows an existing crack, occurred early on in all the analyses. This crack propagates towards the base of the wall in a fashion very similar to the existing crack at the structure. In general, the investigated loading directions show that the existing damage in the tower would correlate very well with the damage caused by an earthquake with a principal component in the east–west direction. For the rest of the loading directions, the northern part of the structure also developed significant cracks. It is noted that all studied cases exhibit early horizontal cracking at the base of the external walls, which was not observed during the visual inspection. The cracking at the base also appeared in the fundamental load combination with wind, soil, dead and live loads, which led to the conclusion that the assumed foundation level was overly conservative, as the damage observed in the model was not observed in the real structure.

Two scenarios for differential soil settlements were considered by applying incremental vertical (Figure 23 bottom) and diagonal displacements over a portion of the base of the eastern walls of the tower that is separated from the rest of the structure by two existing rock joints. Displacements were imposed at the base of the easternmost wall. In both loading scenarios, the cracking pattern was similar to that observed in the real structure. Based on the above analyses, it can be concluded that a large part of the existing damage is due to a differential soil settlement at the base of the eastern walls.

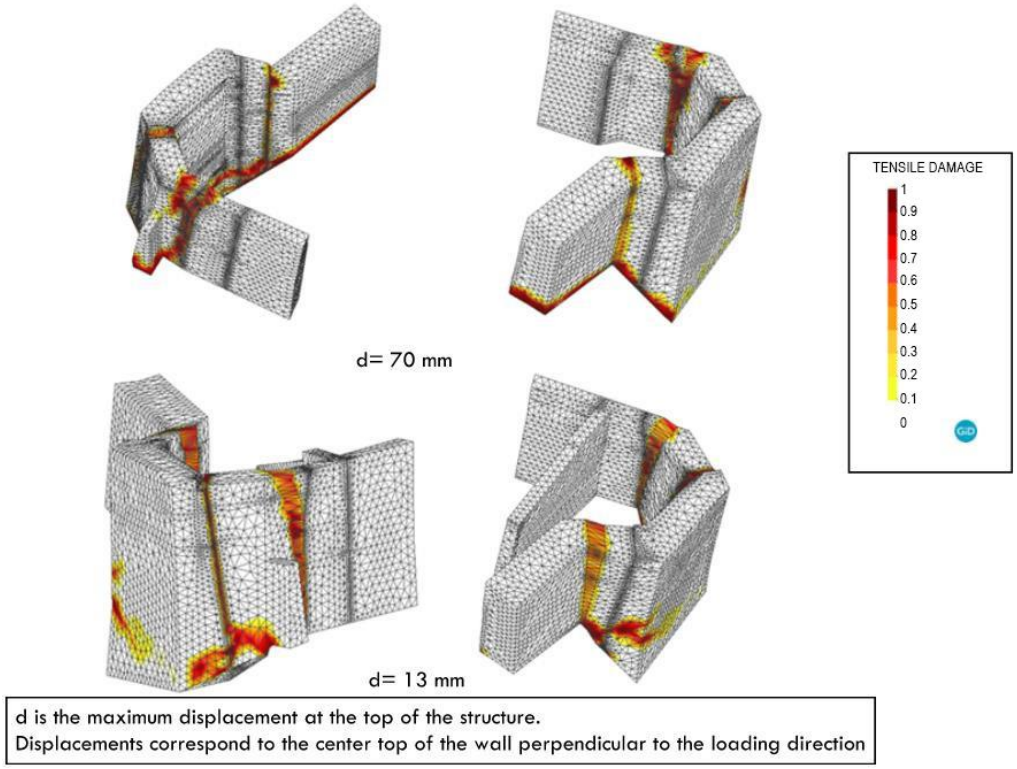

Figure 23. (**top**) Tensile damage in the pushover analysis carried out in the east–west direction (deformation ×50); (**bottom**) tensile damage after imposed vertical movement (deformation ×50).

Seismic Assessment

In-depth geological and structural studies concluded that the extensive cracking is most likely due to geological movement of the conglomerate rocks below the foundation level. Nevertheless, the numerical analyses show that in its current deteriorated state, the structure is vulnerable to further damage from earthquakes. The rear wall was identified as a weak point of the tower, since the capacity of the structure was significantly lower when the rear wall was included in the analysis. According to the reference peak ground acceleration values assumed, there is a 1.9% chance of having a seismic event in the next 10 years that would trigger the instability of this wall. The analyses also showed that the rear wall is a key element for providing stability to walls NW1 and NW2 (Figure 24). Figure 25 shows an example of the results obtained from the numerical pushover analysis and the assessment carried out following the N2 method. The results show that a retrofitting intervention improving the capacity of the rear wall can be a good strategy for increasing the overall capacity of the tower.

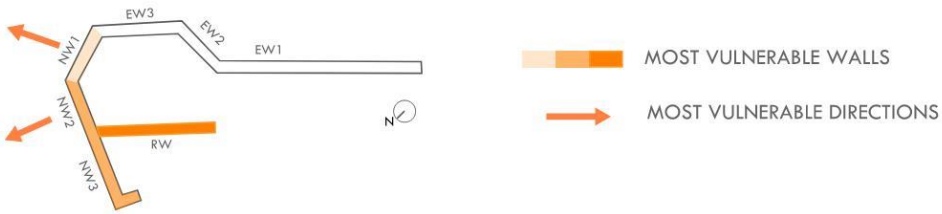

Figure 24. Location of the most vulnerable walls and loading directions.

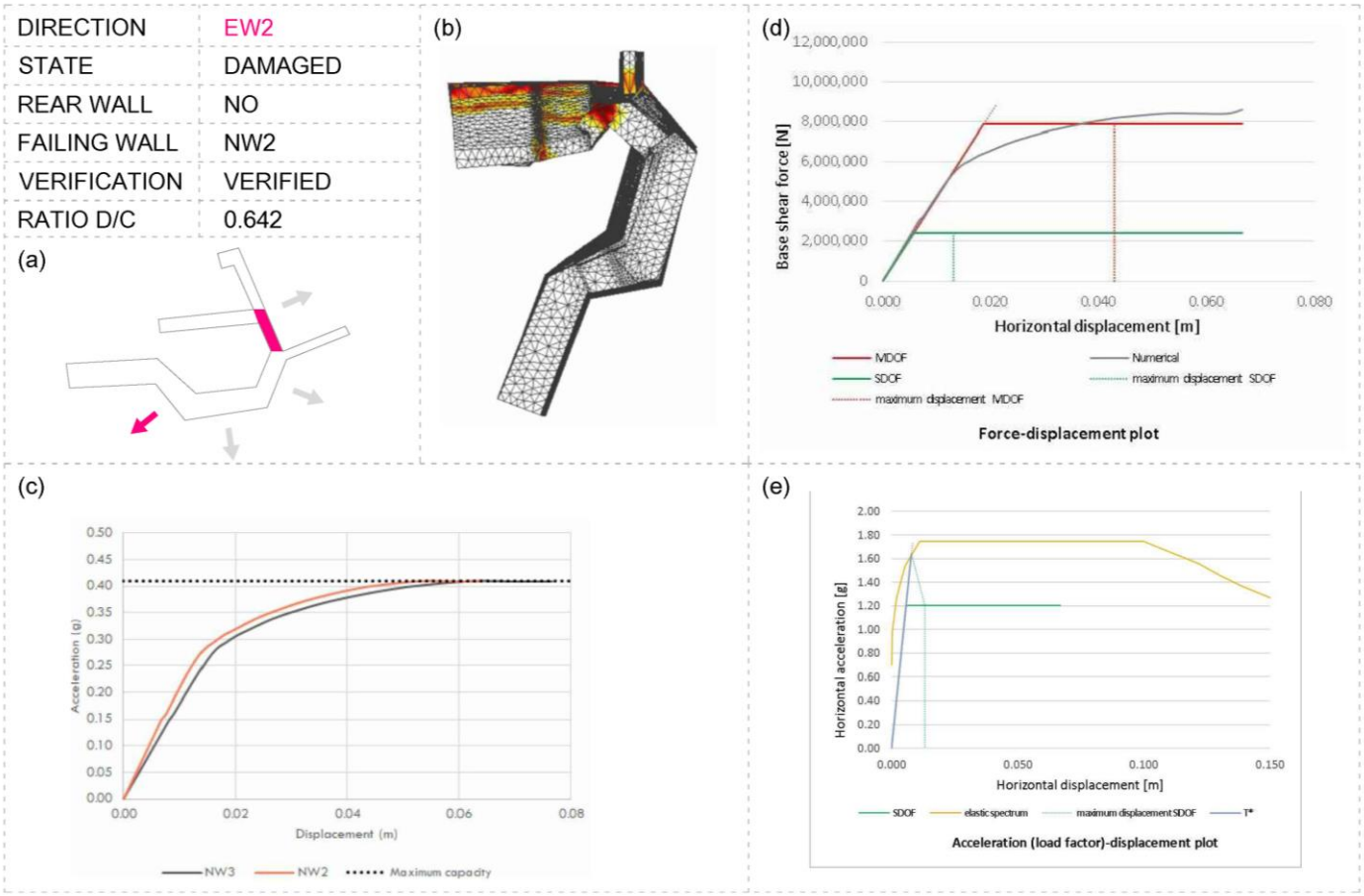

Figure 25. Example of seismic assessment of wall NW2 for loading applied orthogonal to EW2 in the existing condition without incorporating the rear wall: (**a**) pushover direction and the failing wall; (**b**) failure mode in the finite element model; (**c**) acceleration-displacement plot for the walls NW2 and NW3, as well as the maximum acceleration reached; (**d**) compliant N2 method verification as a force-displacement plot, with numerical model curve, the bilinear curves for a multiple degree of freedom system (MDOF) and a single degree of freedom system (SDOF), as well as the corresponding target displacements estimated according to EC8; (**e**) acceleration-displacement plot used to determine the target displacement for the equivalent SDOF system, according to EC8.

Additionally, the assessment of the tower walls in their original undamaged condition showed that the presence of cracks and areas of degraded masonry significantly impacts the seismic performance of the structure. The results suggest that if the structure is composed of masonry in good condition, it can withstand code-required loads as the walls are well connected. Therefore, a decision to restore the continuity in the masonry using grout injection was made. The three-fold retrofitting intervention addressed all the main causes of concern, namely the rear wall, the masonry quality and the conglomerate strata on which the tower is supported.

6. Intervention

Intervention criteria were adapted to obtain the desired level of structural safety while considering the high cultural value of the structure as a World Heritage site. These criteria were mainly minimal intervention, respect for traditional materials and skills, sustainability, monitoring prior to intervention, compatibility, cost efficiency and ease of maintenance. The geological intervention was designed to provide a geological stabilization solution that could be implemented with locally available equipment. The design of the structural intervention was developed assuming stabilized geological conglomerate blocks below

the masonry walls. The stabilization of the conglomerate blocks prior to any structural intervention is essential to ensure the efficacy of the latter.

6.1. Geotechnical Intervention: Ground Stabilization

Numerical analyses were carried out to study anchoring solutions and their layout in the conglomerate layer. The failure surfaces that were previously detected in the model of the existing structure were not observed in the models of the retrofitted structure. An example of this, extracted from analyses carried out at a location at the southern end of the castle, can be seen in Figure 26.

The main interventions proposed were drilling and pinning the rock to solid substrate and injecting mortar or concrete into the fissures, joints and cavities below the castle to fill the voids. Netting was also designed and recommended to secure to the rock to prevent rock from falling on the road below. Although the netting is visually obtrusive, its long-term impact on the aesthetical appearance of the site will be minimized with the formation of a patina and vegetation growth. The removal of several large rock blocks, which pose life-threatening risks, will not impact the Outstanding Universal Value (OUV).

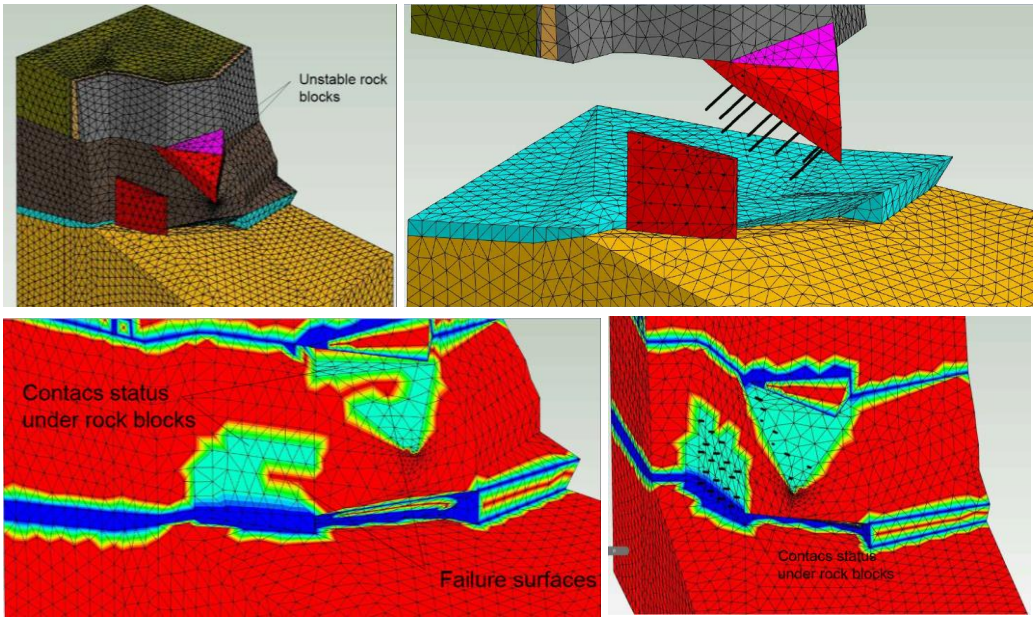

Figure 26. Design of geological intervention at the rock blocks at the southern end of the castle, similar to the ones carried out at the location below the tower: (**top**) location of unstable rocks, where different colours indicate different material properties, such as masonry, soil and rocks (**left**), and proposed anchors (**right**); (**bottom**) comparison of contact status under the rock blocks before and after the introduction of anchors at the southern end of the castle. Red areas within the annotated contact surfaces indicate the presence of failure areas.

6.2. Structural Intervention: Seismic Retrofitting

The geometry of the FE model used in the structural safety assessment of the current condition was updated to incorporate the effects of different retrofitting solutions, namely: (i) masonry injection, considering an upper and lower bound estimation of the improved masonry material properties; (ii) crack repair; and (iii) construction of buttresses at the rear wall (RW).

Modelling of the Intervention

The results of the analyses on the existing structure indicated that the foundation was shallower than what was initially assumed. Hence, the model was updated to increase the

height of the foundation level to match the uppermost conglomerate rock level that was observed on site.

In the first set of analyses, the effect of masonry consolidation and grout injections was evaluated by improving the properties of the masonry. Two scenarios were considered: (1) lower-bound scenario, with a 30% increase in the Young's Modulus of low masonry and a 20% increase for all other masonry types; and (2) upper-bound scenario, with a 50% increase in the Young's Modulus of low masonry and a 40% increase for all other masonry types. Despite greatly improving the capacity, ductility and ultimate displacement of the structure, masonry injection alone was not sufficient to improve the structural performance under code-required loads. Even with the improvement in the masonry properties, the collapse of the rear wall was still the main failure mechanism.

The next set of analyses incorporated the effect of repairing and stitching of the existing cracks. This strengthening technique involves partially reconstructing the masonry surrounding the cracks and grouting. The intervention was incorporated in the model by "closing" the cracks that were previously modelled i.e., adopting material properties that are 80% of the improved masonry properties adjacent to the crack location. In the cases where masonry of different quality was present on each side of the crack, the properties of the crack were based on the lower-quality masonry.

Table 3 shows the nonlinear material properties of the different types of masonry considered in the numerical model of the retrofitted structure. The nonlinear material properties for the masonry were computed based on the updated values of Young's Modulus, using correlations described in Section 4.2.2.

Table 3. Nonlinear material properties of the different qualities of masonry considered in the numerical model.

Masonry	E [N/mm^2]		f_c [N/mm^2]		f_t [N/mm^2]		G_{ft} [N/mm]		G_{fc} [N/mm]		ρ [kg/m^3]
	Lower Bound	Upper Bound	Lower Bound	Upper Bound	Lower Bound	Upper Bound	Lower Bound	Upper Bound	Lower Bound	Upper Bound	
"Original"	3120	3640	5.70	6.60	0.28	0.33	0.017	0.018	9.1	10.6	2100
"Medium"	1680	1960	3.10	3.60	0.15	0.18	0.011	0.012	4.9	5.7	2100
"Low"	910	1050	1.70	1.90	0.07	0.08	0.007	0.008	2.6	3.1	2000
"Restored"	4320	5040	7.90	9.20	0.39	0.46	0.021	0.023	12.6	14.7	2100
"Rear wall"	2640	3080	4.80	5.60	0.24	0.28	0.015	0.016	7.7	9.0	2000

For the strengthening of the rear wall, which is the most vulnerable element of the tower, the addition of buttresses was considered to be the most suitable approach to improve the performance of the wall. Two different geometries were considered (Figure 27): (A) two buttresses with base dimensions of 1 m × 1 m; (B) two buttresses with base dimensions of 1.2 m × 2.6 m and 1.2 m × 2.15 m. The height of the buttress located closer to the NW2 is 5.6 m and the height of the buttress closer to the free end is 4.5 m. The material properties adopted for the buttresses were assumed to match the lower-bound estimate of the material properties of the retrofitted RW.

The results of the comparative analyses concluded that the type A buttresses, which are smaller, were adequate to prevent the rear wall from collapsing. The addition of the buttresses also results in ductile failure modes for most of the loading directions and the structure was able to withstand much larger ultimate displacements. An example of the change in failure mode can be observed in Figure 28, where the failure mode of the existing structure (on the left) is the out-of-plane failure of RW and the failure mode changes to the out-of-plane failure of NW3 (on the right) in the retrofitted condition.

In the retrofitted configuration, the most vulnerable point observed was the connection between NW2 and NW3. Since this location is partially a construction joint between the different phases of the tower, filing the joint will impact the authenticity of the structure. Hence, an alternative strengthening solution that consists of restitching the interior face

of the wall and installing recessed hidden fiberglass bars within the external wythe of the wall was recommended.

In general, the maximum horizontal acceleration, deformation capacity and ductility were found to increase in the retrofitted condition for all directions of analysis. The increase in the maximum horizontal acceleration ranged between 45% and 100%, depending on the loading direction.

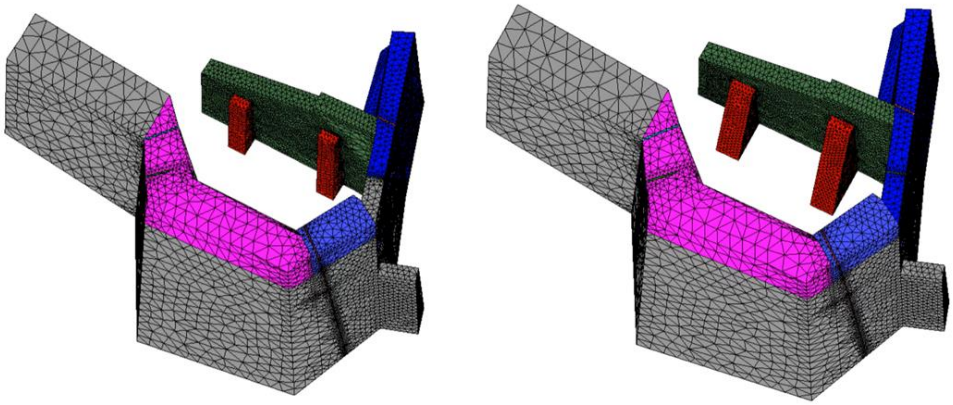

(**a**) (**b**)

Figure 27. View of the mesh in GID 14, showing the two different configurations of buttresses: (**a**) buttress type A; (**b**) buttress type B.

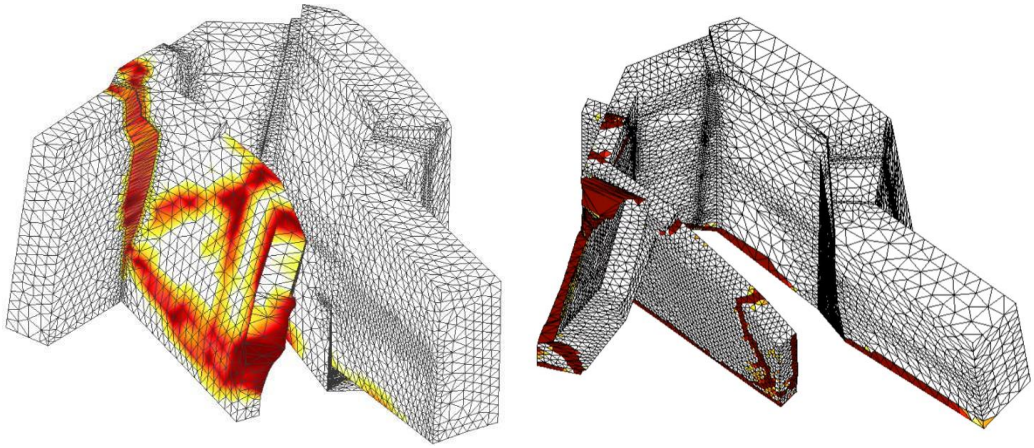

Figure 28. Comparison of tensile damage distribution and deformations for the pushover analyses in EW2 direction considering: (**left**) damaged model with rear wall and (**right**) retrofitted model with lower-bound injections and small buttresses type A. (deformation ×40).

An important aspect that greatly influences the seismic assessment of structures is the selection of the appropriate importance factor γ_I (see Section 5.1). The seismic assessment was originally carried out by conservatively assuming that the castle is a category IV structure, with $\gamma_I = 1.4$, which significantly increases seismic demands. However, World Heritage Sites are not explicitly mentioned within category IV structures of EN 1998-1 [25]. Large seismic demands call for a more invasive intervention, which, in turn, would require more invasive solutions that alter the authenticity of the tower. For this reason, the decision to use an importance category II (ordinary buildings) was taken.

This approach is common practice in heritage engineering and the Guidelines for the Application of the Seismic Ordinance to the Cultural Heritage [39], published by the Italian Ministry of Culture and Tourism, allows practitioners to use reduced seismic demands in Cultural Heritage Buildings to adapt to the building's need.

Using this seismic demand with an importance factor $\gamma_I = 1.0$ allowed the retrofitted structure to comply with the target displacements required by the Eurocode with just the use of lime injections, masonry buttresses and crack stitching. These interventions can potentially improve the results of the seismic assessment up to 10-times in some of the loading directions, as indicated by the results of the finite element analyses.

7. Conclusions

The present paper shows the process and methodology chosen to carry out a seismic retrofitting project of a section of the World Heritage site of Gjirokastra. The paper also demonstrates that all the steps in the process were integral to the success of the project.

In the absence of building drawings and documentation, the geometry of the building was determined by a combination of visual inspection, laser scanning and photogrammetry. Sonic tests, material testing on loose units and GPR were instrumental in estimating material properties and understanding the wall morphology. The dynamic identification tests were useful to calibrate the numerical model and provided a means to characterize the behaviour of the cracks in the masonry. The incorporation of the information obtained from these sources allowed us to gain confidence in the ability of the model to simulate the behaviour of the real structure and to determine the cause of the observed damage. Similar to the process followed for the superstructure, the non-destructive geotechnical tests provided information on the underlying conditions at the site and acted as a feeder for the finite element model, which was used to evaluate different strengthening solutions.

The comparison between the seismic performance of the different models allowed us to make an informed decision to determine the most optimal retrofitting solution, not only in terms of safety, but also taking into account respect to the authenticity of the structure, avoiding a more invasive approach. The proposed methodology can be tailored to other heritage sites that demand such a non-invasive approach to guarantee the structural safety while preserving the heritage values.

Author Contributions: Conceptualization, J.A.A.C., M.N.G. and F.M.R.; methodology, J.A.A.C., M.N.G., J.O., S.S. and F.M.R.; software, S.S.; validation, J.A.A.C., M.N.G., J.O., S.S. and F.M.R.; formal analysis, F.M.R., M.N.G., J.O., S.S., F.G., C.A. and J.A.A.C.; investigation, J.A.A.C., M.N.G., I.M.C., F.M.R., J.O., S.S., F.G. and C.A.; resources, J.A.A.C., F.M.R., J.O., S.S., F.G., C.A. and M.N.G.; writing—original draft preparation, J.O., F.M.R. and M.N.G.; writing—review and editing, F.G., C.A., S.S., J.O. and M.N.G.; visualization, F.M.R., M.N.G., J.O., S.S., F.G. and C.A.; supervision, J.A.A.C., F.M.R., J.O. and S.S.; project administration, J.A.A.C. and M.N.G.; funding acquisition, J.A.A.C. All authors have read and agreed to the published version of the manuscript.

Funding: This project was funded by the Albanian Development Fund and the World Bank by the project "Identification, Design of prioritized measures to address urgent safety concerns and prevent loss of heritage structures in the Castle of Gjirokastra".

Institutional Review Board Statement: Not applicable.

Informed Consent Statement: Not applicable.

Data Availability Statement: Not applicable.

Acknowledgments: The work covered in this publication is part of a larger mulidisciplinary project addressing the totality of the castle of Gjirokastra. The project goal was to identify and design prioritized measures to address urgent safety concerns and prevent loss of heritage structures in the castle of Gjirokastra. The outcomes were the preparation of a conservation plan (including assessment of significance; condition assessment; identification of all necessary conservation interventions; methodology concerning intervention selection; intervention prioritization and costing; and intervention scheduling) and detailed conservation designs for the selected conservation interventions. The project was developed by the joint venture formed by CHwB Albania and Proskene Conservation and Cultural Heritage as consultants. The construction of the designed interventions was being carried out at the moment in which this article was finished. The authors would like to thank their partners and collaborators during the project, team leader Rand Eppich and the architects Lejla Hadzic and Elena Mamani from Cultural Heritage without Borders Albania, for all the work carried

out during the development of the joint project that helped the engineering team to better understand the structure, such as historical research, surveying and inspection. Part of the seismic assessment was carried out during COVID-19 outbreak lockdown and having them as partners was crucial for the success of the engineering interventions.

Conflicts of Interest: The authors declare no conflict of interest.

References

1. ICOMOS/ISCARSAH (International Council on Monuments and Sites/International Scientific Committee on the Analysis and Restoration of Structures of Architectural Heritage) Committee. *Recommendations for the Analysis, Conservation and Structural Restoration of Architectural Heritage*; ICOMOS: Paris, France, 2005.
2. Aguilar, A. *Preservation Brief 41: The Seismic Rehabilitation of Historic Buildings*; National Park Service, Historical Preservation Services, US Department of the Interior: Washington, DC, USA, 2016.
3. Roca, P.; Cervera, M.; Gariup, G. Structural analysis of masonry historical constructions. Classical and advanced approaches. *Arch. Comput. Methods Eng. 2010 17*, 299–325. [CrossRef]
4. Mallardo, V.; Malvezzi, R.; Milani, E.; Milani, G. Seismic vulnerability of historical masonry buildings: A case study in Ferrara. *Eng. Struct.* **2008**, *30*, 2223–2241. [CrossRef]
5. Saloustros, S.; Pelà, L.; Roca, P.; Portal, J. Numerical analysis of structural damage in the church of the Poblet Monastery. *Eng. Fail. Anal.* **2015**, *48*, 41–61. [CrossRef]
6. Castellazzi, G.; D'Altri, A.M.; de Miranda, S.; Ubertini, F. An innovative numerical modeling strategy for the structural analysis of historical monumental buildings. *Eng. Struct.* **2017**, *132*, 229–248. [CrossRef]
7. Aranha, C.A.; Menon, A.; Sengupta, A. Determination of the causative mechanism of structural distress in the Presidential Palace of India. *Eng. Fail. Anal.* **2019**, *95*, 312–331. [CrossRef]
8. Greco, F.; Lourenco, P.B. Seismic assessment of large historic vernacular adobe buildings in the Andean Region of Peru. Learning from Casa Arones in Cusco. *J. Build. Eng.* **2021**, *40*, 102341. [CrossRef]
9. Dinani, A.T.; Destro Bisol, G.; Ortega, J.; Lourenço, P.B. Structural Performance of the Esfahan Shah Mosque. *J. Struct. Eng.* **2021**, *147*, 05021006. [CrossRef]
10. D'Ambrisi, A.; Mariani, V.; Mezzi, M. Seismic assessment of a historical masonry tower with nonlinear static and dynamic analyses tuned on ambient vibration tests. *Eng. Struct.* **2012**, *36*, 210–219. [CrossRef]
11. Costa, C.; Ribeiro, D.; Jorge, P.; Silva, R.; Arêde, A.; Calçada, R. Calibration of the numerical model of a stone masonry railway bridge based on experimentally identified modal parameters. *Eng. Struct.* **2016**, *123*, 354–371. [CrossRef]
12. Torelli, G.; D'Ayala, D.; Betti, M.; Bartoli, G. Analytical and numerical seismic assessment of heritage masonry towers. *Bull. Earthq. Eng.* **2019**, *18*, 969–1008. [CrossRef]
13. Spoldi, E.; Ippolito, I.; Stella, A.; Russo, S. Non-destructive techniques for structural characterization of cultural heritage: A pilot case study. *Struct. Control. Health Monit.* **2021**, *28*, e2820. [CrossRef]
14. Oller, P.; Gonzalez, M.; Pinyol, J.; Marturià, J.; Martínez, P. Geohazards Mapping in Catalonia. *J. Torrent Avalanche Landslide Rock Fall Eng.* **2011**, *74*, 148–155.
15. Achache, J.; Fruneau, B.; Delacourt, C. Applicability of SAR interferometry for operational monitoring of landslides. In Proceedings of the Second ERS Applications Workshop, London UK, 6–8 December 1995; pp. 165–168.
16. Binda, L.; Saisi, A.; Tiraboschi, C. Investigation procedures for the diagnosis of historic masonries. *Constr Build Mater* **2000**, *14*, 199–233. [CrossRef]
17. Miranda, L.F.; Rio, J.; Miranda Guedes, J.; Costa, A. Sonic Impact Method—A new technique for characterization of stone masonry walls. *Constr. Build Mater.* **2012**, *36*, 27–35. [CrossRef]
18. Trifunac, M.D.; Todorovska, M.I.; Manic, M.I.; Bulajic, B. Variability of the fixed-base and soil–structure system frequencies of a building—The case of Borik-2 building. *Struct. Control Health Monit.* **2010**, *17*, 120–151. [CrossRef]
19. Bulajic, B.D.; Todorovska, M.I.; Manic, M.I.; Trifunac, M.D. Structural health monitoring study of the ZOIL building using earthquake records. *Soil Dyn. Earthq. Eng.* **2020**, *133*, 106105. [CrossRef]
20. Brinkers, R.; Kirkegaard, P. Special issue on operational modal analysis. *Mech. Syst. Signal Process.* **2001**, *24*, 1209–1212. [CrossRef]
21. Peeters, B.; De Roeck, G. Reference-based stochastic subspace identification for output-only modal analysis. *Mech. Syst. Signal Process.* **1999**, *13*, 855–878. [CrossRef]
22. SVS. *ARTeMIS Extractor Pro User's Manual, Release 6.0. Structural Vibration Solutions*; SVS: Aalborg, Denmark, 2019.
23. Pastor, M.; Binda, M.; Harčarik, T. Modal assurance criterion. *Procedia Eng.* **2012**, *48*, 543–548. [CrossRef]
24. Ewins, D.J. *Modal Testing: Theory, Practice and Applications*, 2nd ed.; Research Studies Press: Baldock, UK, 2000.
25. *EN 1998-1*; Eurocode 8: Design of Structures for Earthquake Resistance. Part 1: General Rules, Seismic Action and Rules for Buildings. European Committee for Standardisation (CEN): Brussels, Belgium, 2005.
26. Freddi, F.; Novelli, V.; Gentile, R.; Velieu, E.; Andreev, S.; Andonov, A.; Greco, F.; Zhukelu, E. Observations from the 26th November 2019 Albania earthquake: The earthquake engineering feld investigation team (EEFIT) mission. *Bull. Earthq. Eng.* **2021**, *19*, 2013–2044. [CrossRef]

27. *KTP-N.2-89, 1989*; Technical Aseismic Regulations. Publication of Academy of Sciences and Ministry of Constructions: Tirana, Albania, 1989. (In Albanian)
28. Fajfar, P. A Nonlinear Analysis Method for Performance-Based Seismic Design. *Earthq. Spectra* **2000**, *16*, 573–592. [CrossRef]
29. 29. *EN 1990*; Eurocode—Basis of Structural Design. European Committee for Standardisation (CEN): Brussels, Belgium, 2002.
30. Brocher, T.M. Empirical relations between elastic wavespeeds and density in the Earth's crust. *Bull. Seismol. Soc. Am.* **2005**, *95*, 2081–2092. [CrossRef]
31. Karanikoloudis, G.; Lourenço, P.B. Structural assessment and seismic vulnerability of earthen historic structures. Application of sophisticated numerical and simple analytical models. *Eng. Struct.* **2018**, *160*, 488–509. [CrossRef]
32. Pešić, N.; Živanović, S.; Dennis, J.; Hargreaves, J. Experimental and finite element dynamic analysis of incrementally loaded reinforced concrete structures. *Eng. Struct.* **2015**, *103*, 15–27.
33. Lollino, G.; Giordan, D.; Marunteanu, C.; Christaras, B.; Yoshinori, I.; Margottini, C. *Engineering Geology for Society and Territory–Volume 8: Preservation of Cultural Heritage*; Springer: New York, NY, USA, 2015; pp. 1–584.
34. FEMA. *Evaluation of Earthquake Damaged Concrete and Masonry Wall Buildings. Basic Procedures Manual, Management*; FEMA: Washington, DC, USA, 1998.
35. Angelillo, M.; Lourenço, P.B.; Milani, G. *Mechanics of Masonry Structures*; Springer: New York, NY, USA, 2014; Volume 551.
36. Faria, R.; Oliver, J.; Cervera, M. A strain-based plastic viscous-damage model for massive concrete structures. *Int. J. Solids Struct.* **1998**, *35*, 1533–1558. [CrossRef]
37. Saloustros, S.; Pelà, L.; Cervera, M.; Roca, P. Finite element modelling of internal and multiple localized cracks. *Comput. Mech.* **2017**, *59*, 299–316. [CrossRef]
38. Petracca, M.; Pelà, L.; Rossi, R.; Oller, S.; Camata, G.; Spacone, E. Regularization of first order computational homogenization for multiscale analysis of masonry structures. *Comput. Mech.* **2016**, *57*, 257–276. [CrossRef]
39. Ministero per i Beni e le Attività Culturali. *Linee Guida per la Valutazione e Riduzione del Rischio Sismico del Patrimonio Culturale*; Ministero per i Beni e le Attività Culturali: Rome, Italy, 2021; ISBN 978-88-492-1165-8.